Multiband mean-field theory of the d + ig superconductivity scenario in Sr_2RuO_4

Andrew C. Yuan¹, Erez Berg, and Steven A. Kivelson¹ ¹Department of Physics, Stanford University, Stanford, California 93405, USA ²Department of Condensed Matter Physics, Weizmann Institute of Science, Rehovot 7610001, Israel

(Received 30 September 2022; revised 16 June 2023; accepted 20 June 2023; published 6 July 2023)

Many seemingly contradictory experimental findings concerning the superconducting state in Sr₂RuO₄ can be accounted for on the basis of a conjectured accidental degeneracy between two patterns of pairing that are unrelated to each other under the (D_{4h}) symmetry of the crystal: a $d_{x^2-y^2}$ -wave (B_{1g}) and a $g_{xy(x^2-y^2)}$ -wave (A_{2g}) superconducting state. In this paper, we propose a generic multiband model in which the g-wave pairing involving the xz and yz orbitals arises from second-nearest-neighbor BCS channel effective interactions. Even if timereversal symmetry is broken in a d + ig state, such a superconductor remains gapless with a Bogoliubov Fermi surface that approximates a (vertical) line node. The model gives rise to a strain-dependent splitting between the critical temperature T_c and the time-reversal symmetry-breaking temperature T_{TRSB} that is qualitatively similar to some of the experimental observations in Sr₂RuO₄.

DOI: 10.1103/PhysRevB.108.014502

I. INTRODUCTION

For more than two decades, Sr₂RuO₄ was generally believed to be a chiral p-wave superconductor (SC) mainly due to a compelling narrative based on early experiments [1–5]. The extreme sensitivity of the superconducting state to impurities [6] unambiguously establishes that it is an unconventional SC, and various experiments confirm that the gap is nodal [7,8]. However, recent nuclear magnetic resonance (NMR) experiments have seemingly ruled out triplet pairings of any sort [9-11].

Further constraints on the symmetry of the SC order can be inferred from a variety of experiments. Elastocaloric data [12] obtained when the Fermi surface is tuned through a Lifshitz transition strongly suggest that the SC gap is nonvanishing at the Van Hove points. Moreover, ultrasound experiments, taken at face value, suggest a two-component order parameter with highly constrained symmetries [13,14]: A discontinuity in the c_{66} shear modulus implies that the only possibilities consist of the innately two-dimensional irrep d_{xz} - d_{yz} (E_g) [15–21] or an accidental degeneracy between two distinct one-dimensional irreps whose tensor product has B_{2g} symmetry, i.e., $d_{x^2-y^2}$ and g [22–26] or s and d_{xy} [27,28]. Evidence [29,30] of time-reversal symmetry (TRS) breaking at or slightly below T_c provides further evidence of a two-component order parameter.

That the Fermi surface of Sr₂RuO₄ is quasi-twodimensional, i.e., it consists of three cylindrical sheets corresponding to the α , β , and γ bands, makes it seem unlikely that the SC order parameter has strong inter-layer pairing in the vertical z direction, which provides an additional strong reason to exclude the possibility of d_{xz} - d_{yz} (E_g) pairing. This is further supported by the lack of a visible discontinuity in the $(c_{11} - c_{12})/2$ (B_{1g}) shear modulus [13]. Conversely, an accidental degeneracy between distinct irreps requires a certain degree of fine tuning so that the critical temperature T_c is roughly equal to the TRS breaking temperature T_{TRSB} , i.e., $T_c \approx T_{\text{TRSB}}$. However, this requires only one degree of

fine tuning and thus could plausibly arise in a small subset of SC materials.

In our recent works [22,23], we preferred the $d_{x^2-y^2}+ig$ pairing symmetry over the $s + id_{xy}$ wave, mainly due to experimental observations of line nodes in the SC gap function [7,8,31]. Indeed, in a single-band model, d + ig pairing leaves symmetry-protected line nodes along the diagonal directions (110), (110), while $s + id_{xy}$ pairing would require an extra degree of fine tuning, i.e., a $(s + id_{xy})$ -wave SC is generically fully gapped. However, a perturbative study of the effective interaction based on a "realistic" multiband model of the electronic structure of Sr₂RuO₄ concluded that the leading instabilities are in the s and d_{xy} channels [27,28]; this result raises issues concerning the "naturalness" of the $d_{x^2-y^2}+ig$ SC state. In particular, within a single band on a square lattice, the pair wave function in a g-wave state vanishes at all distances shorter than fourth-nearest neighbors, and thus seemingly requires unnaturally long-range interactions.

To address this problem, we consider a generic multiband microscopic BCS model in which the results follow largely from symmetry considerations. In this model, the g wave always lives primarily on the α and β bands, which derive from the symmetry-related xz and yz Ru orbitals. There are two reasons for this: (1) g-wave pairing is strongly disfavored in the xy band in that the pair wave function vanishes where the density of states is largest in the vicinity of the Van Hove points. (2) Coupling between the xz and yz bands permits g-wave pairing to be induced by second-nearest-neighbor effective interactions, 1 i.e., much shorter range than is required

¹Note: The interactions here should be viewed as effective interactions. However, so long as any fluctuations that mediate such interactions are far from critical, the resulting effective interactions will be short ranged in space and time, as assumed here. For instance, the correlation length associated with short-range spin-density wave correlations ($\Delta q = 0.13 \,\text{Å}^{-1}$) seen in neutron scattering [48] has

in a single-band context. Conversely, the $d_{x^2-y^2}$ component is strongest on the xy band.

As a consequence, the model readily accounts for the recently observed uniaxial stress dependence of the splitting of the critical temperature T_c from the time-reversal symmetry (TRS) breaking T_{TRSB} [29]. As we show via microscopic Bogoliubov-de Gennes (BdG) calculations (Fig. 3), application of uniaxial stress has little effect on T_c until it is sufficiently strong to trigger a sharply peaked enhancement close to the critical strain at which the xy band crosses a Van Hove point, leading to a divergent density of states (DOS) [12,32,33]. In contrast, across this Lifshitz transition, the xzand yz bands are only slightly distorted (an asymmetry of \sim 2%) [29] and thus the g-wave component of the order parameter is largely unaffected, resulting in a T_{TRSB} that is only weakly strain dependent. (The strain dependence would be quite different for a putative $(s + id_{xy})$ -wave state, in which both components sit on all bands.) Within our model, the approximate degeneracy between the d- and g-wave components persists in the presence of symmetry-breaking shear strain. However, it is lifted by isotropic strain and leads to a linear increase in T_c ; this effect has not been detected in recent experiments [34]. How to reconcile this observation with our d + ig proposal remains unresolved at present.

Regarding the nodal structure, we show that the symmetry-protected line nodes along the diagonal planes (110), (110) anticipated in the single-band model extend into Bogoliubov Fermi surfaces (FS) in the general multi-band $d_{x^2-y^2}+ig$ state. The Bogoliubov FSs are extended in the k_z direction and consist of narrow ellipses for generic k_z , that pinch into point nodes in the $k_z=0$ and π planes. The pinching off at $k_z=0$ and π is due to a combination of the mirror symmetries $\mathcal{M}_z:z\mapsto -z$ and $\mathcal{M}_{xy}:x\leftrightarrow y.^2$ In practice, such Bogoliubov Fermi surfaces would exhibit behavior characteristic of line nodes (as is observed experimentally [7,8,31]), except at extremely low temperatures.

II. MICROSCOPIC ANALYSIS

A. Setup

Unless otherwise specified, we will consider a twodimensional (2D) model, corresponding to a single RuO₂ plane. [We we will consider the effects of three-dimensional

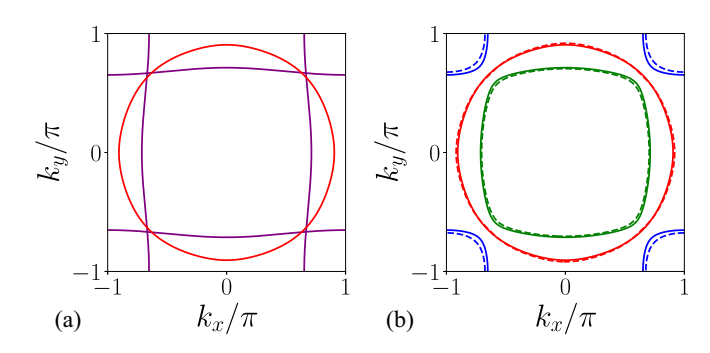


FIG. 1. (a) Fermi surfaces (FS) computed in the absence of hybridization and spin-orbit (SO) coupling. (b) FS including the effect of hybridization between the xz, yz bands but no SO (solid lines), and with both hybridization and SO (dashed lines). Here interplane dispersion is neglected; numerical parameters are given in Appendix A.

(3D) dispersion in the discussion of the nodal structure.] We will always restrict our attention (for reasons already discussed) to gap functions that are even with respect to both parity \mathcal{P} and under mirror symmetry \mathcal{M}_z . This leaves us with only one-dimensional irreps of the point group D_{4h} , i.e., (s,d,d',g)-wave pairings $(A_{1g},B_{1g},B_{2g},A_{2g},$ respectively).

B. Normal state

Let us first consider the normal state $\Delta=0$ where the Hamiltonian is

$$\mathcal{H}_{0} = \mathcal{H}_{intra} + \mathcal{H}_{hybrid} + \mathcal{H}_{SO},$$

$$\mathcal{H}_{intra} = \sum_{\mathbf{k}\nu s} \varepsilon_{\nu}(\mathbf{k}) \psi_{\nu s}^{\dagger}(\mathbf{k}) \psi_{\nu s}(\mathbf{k}),$$

$$\mathcal{H}_{hybrid} = \sum_{\mathbf{k}s} \varepsilon_{h}(\mathbf{k}) (\psi_{xs}^{\dagger}(\mathbf{k}) \psi_{ys}(\mathbf{k}) + H.c),$$

$$\mathcal{H}_{SOC} = \sum_{\mathbf{k}\nu\nu'ss'} \varepsilon_{SOC}(\mathbf{k}) \psi_{\nu s}^{\dagger}(\mathbf{k}) \psi_{\nu's'}(\mathbf{k}) \mathbf{l}_{\nu\nu'} \cdot \boldsymbol{\sigma}_{ss'}.$$
 (1)

The first term $\mathcal{H}_{\text{intra}}$ represents the dispersion of each orbital v = x, y, z (for d_{yz}, d_{zx}, d_{xy} respectively), while the second term $\mathcal{H}_{\text{hybrid}}$ is the spin-conserving hybridization between the x, y bands and generates the α, β bands shown in Fig. 1, where $\varepsilon_h(\mathbf{k})$ characterizes the strength of hybridization between the x, y bands.³ The third term represents the spin-orbit coupling (SOC) where $I^{\mu}_{vv'} = -i\epsilon_{vv'\mu}$. The specific parametrizations of $\varepsilon_v(\mathbf{k}), \varepsilon_h(\mathbf{k})$, and $\varepsilon_{\text{SOC}}(\mathbf{k})$ used in our calculations are given in Appendix A.

In the normal state, $\mathcal{P}, \mathcal{M}_z, \mathcal{T}$ are all preserved. The single-particle space can thus be decomposed into the eigenspaces of $\mathcal{M}_z = \pm i$, with ordered basis $|+\rangle \equiv$

a correlation length that is $1/(a\Delta q) \approx 2$ lattice constants, where a = 3.85 Å is the in-plane lattice spacing.

²In general, mirror symmetry \mathcal{M}_z acts on both on \mathbf{k} space and orbital and spin space M_z so that $\mathcal{M}_z = M_z \otimes (k_z \mapsto -k_z)$. In the $k_z = 0$, π planes, \mathcal{M}_z conserves \mathbf{k} so that $\mathcal{M}_z = M_z$, and thus when the state is even under \mathcal{M}_z , the \mathbf{k} -conserving Hamiltonian is decoupled in the eigenspaces $M_z = \pm i$. Away from the $k_z = 0$, π planes, such a decomposition is not exact and thus the radius of the Bogoliubov Fermi surface is in proportion to the weak coupling between the orbital and spin eigenspaces $M_z = \pm i$. This is not necessarily on the same magnitude as the interplane coupling. Indeed, one could imagine a general 3D Hamiltonian with k_z dependence (due to interplane coupling), but still decoupled in the eigenspaces $M_z = \pm i$ involving only orbital and spin (see Appendix D). This particular scenario would not be enough to induce Bogoliubov Fermi surfaces.

³It should be noted that due to \mathcal{M}_z symmetry, there exists no spin-conserving hybridization between the x, z bands and y, z bands, i.e., $\varepsilon_{x,z} = \varepsilon_{y,z} = 0$. However, in a full 3D model, such hybridization terms are allowed and can give rise to gap functions between the x, z bands and y, z bands, i.e., $\Delta_{x,z}$, $\Delta_{y,z} \neq 0$, even in the absence of spin-orbit coupling. Since Sr_2RuO_4 is quasi-2D, such terms can always be treated perturbatively.

⁴That $\mathcal{M}_z^2 = -1$ is due to its action on the spin sector.

 $(x\uparrow,y\uparrow,z\downarrow)$ and $|-\rangle \equiv (x\downarrow,y\downarrow,-z\uparrow)$, respectively.⁵ The signs are chosen so that the **k**-conserving antiunitary symmetry \mathcal{TP} maps $|+\rangle \mapsto |-\rangle$, and thus the two eigenspaces have equivalent energy levels.⁶ The normal state Hamiltonian is simplified as

$$\mathcal{H}_0 = \sum_{\mathbf{k}, a = \pm} \psi_a^{\dagger}(\mathbf{k}) \hat{\varepsilon}_a(\mathbf{k}) \psi_a(\mathbf{k}),$$

$$\hat{\varepsilon}_{\pm} = \langle \pm | \varepsilon | \pm' \rangle = \begin{bmatrix} \varepsilon_{x} & \varepsilon_{h} \mp i \varepsilon_{SOC} & \varepsilon_{SOC} \\ \varepsilon_{h} \pm i \varepsilon_{SOC} & \varepsilon_{y} & \mp i \varepsilon_{SOC} \\ \varepsilon_{SOC} & \pm i \varepsilon_{SOC} & \varepsilon_{z} \end{bmatrix},$$
(2

where ψ_{\pm}^{\dagger} are the creation operators for the basis $|\pm\rangle$ and $\hat{\varepsilon}_{-}=\hat{\varepsilon}_{+}^{*}$ due to $\mathcal{TP}.^{7}$ Using a multiorbital symmetry analysis (Table II of [19] or Appendix B), the components $\varepsilon_{x}(\mathbf{k}) \pm \varepsilon_{y}(\mathbf{k})$, $\varepsilon_{h}(\mathbf{k})$ must satisfy (S,D,D')-wave (A_{1g},B_{1g},B_{2g}) symmetry in \mathbf{k} space, respectively.⁸

C. BCS state

Since the BCS Hamiltonian is assumed to preserve \mathcal{M}_z , a similar decomposition can be performed on the general multiband particle-hole space. More specifically, particle states $|+\rangle$ and hole states $|-\rangle$ form an ordered basis for the eigenspace $\mathcal{M}_z = +i$, and particle states $|-\rangle$ and hole states $|+\rangle$ for $\mathcal{M}_z = -i$. Let \mathcal{C} denote particle-hole symmetry so that \mathcal{CP} denotes a **k**-conserving antiunitary symmetry [maps $\mathcal{H}(\mathbf{k}) \mapsto -\mathcal{H}(\mathbf{k})$] between the $\mathcal{M}_z = +i \leftrightarrow -i$ eigenspaces. Hence, the BCS Hamiltonian \mathcal{H} in the decoupled eigenspaces $\mathcal{M}_z = \pm i$ have equivalent (opposite signed) energy levels. When TRS \mathcal{T} is preserved, each eigenspace is further doubly (opposite signed) degenerate due to the local unitary symmetry \mathcal{TC} which commutes with \mathcal{M}_z . Therefore, we can use the

TABLE I. The $\eta = \pm$ signs in the table are such that $C(\mathbf{k}) \mapsto \eta C(\mathbf{k}')$ under point-group operation $\mathcal{O} = \mathcal{C}_4, \mathcal{M}_{xy}$ where $\mathbf{k}' \equiv \mathcal{O}^{-1}\mathbf{k}$. The first four components (last five) correspond to singlet (triplet) pairing.

Component $C \setminus \text{Operation } \mathcal{O}$	\mathcal{C}_4	\mathcal{M}_{xy}
Δ_z	+	+
$\Delta_x + \Delta_y$	+	+
$\Delta_x - \Delta_y$	_	_
$\Delta_{x,y} + \Delta_{y,x}$	_	+
$\Delta_{x,y} - \Delta_{y,x}$	+	+
$\Delta_{x,z} + \Delta_{z,x} + i(\Delta_{y,z} - \Delta_{z,y})$	+	+
$\Delta_{x,z} + \Delta_{z,x} - i(\Delta_{y,z} - \Delta_{z,y})$	_	_
$\Delta_{y,z} + \Delta_{z,y} + i(\Delta_{x,z} - \Delta_{z,x})$	_	+
$\Delta_{y,z} + \Delta_{z,y} - i(\Delta_{x,z} - \Delta_{z,x})$	+	_

Nambu spinors $\Psi_{\pm}^{\dagger}(\mathbf{k}) = (\psi_{\pm}^{\dagger}(\mathbf{k}), \psi_{\mp}(-\mathbf{k}))$ to write the BCS Hamiltonian in the following block-matrix form:

$$\mathcal{H} = \sum_{\mathbf{k}, a = \pm} \Psi_a^{\dagger}(\mathbf{k}) H_a(\mathbf{k}) \Psi_a(\mathbf{k}),$$

$$H_{\pm}(\mathbf{k}) = \begin{bmatrix} \hat{\varepsilon}_{\pm}(\mathbf{k}) & \hat{\Delta}_{\pm}(\mathbf{k}) \\ \hat{\Delta}_{\pm}^{\dagger}(\mathbf{k}) & -\hat{\varepsilon}_{\pm}(\mathbf{k}) \end{bmatrix},$$

$$\hat{\Delta}_{+}(\mathbf{k}) = \begin{bmatrix} \Delta_{x} & \Delta_{x,y} & \Delta_{x,z} \\ \Delta_{y,x} & \Delta_{y} & \Delta_{y,z} \\ \Delta_{z,x} & \Delta_{z,y} & \Delta_{z} \end{bmatrix}, \quad \hat{\Delta}_{-} = -\hat{\Delta}_{+}^{T}, \quad (3)$$

where $\hat{\varepsilon}_{\pm}(\mathbf{k})$ is given in Eq. (2). In the case where TRS \mathcal{T} is preserved, $\hat{\Delta}(\mathbf{k})^{\dagger} = \hat{\Delta}(\mathbf{k})^{10}$

D. Symmetries of gap matrix

Using a multiorbital symmetry analysis ([19] or Appendix B), it is straightforward (but a bit complicated) to see that the matrix elements of $\hat{\Delta}(\mathbf{k})$ are mapped under $\pi/2$ rotation \mathcal{C}_4 and $x \leftrightarrow y$ mirror symmetry \mathcal{M}_{xy} (the remaining generators of D_{4h}), in the manner tabulated in Table I. Depending on the overall symmetry of the SC gap, the remaining matrix components must satisfy corresponding symmetries in \mathbf{k} space shown in Table II.

It is worth mentioning that SOC in general mixes (physical) spin-singlet and -triplet pairings. Indeed, the gap matrix $\hat{\Delta} = \hat{\Delta}^{\text{singlet}} + \hat{\Delta}^{\text{triplet}}$ can be decomposed into a singlet component $\hat{\Delta}^{\text{singlet}}$ and a triplet component $\hat{\Delta}^{\text{triplet}}$ (referred to as

⁵Technically, $|\pm\rangle$ are ordered bases for the eigenspaces of $M_z=\pm i$ where M_z is the orbital and spin action of \mathcal{M}_z so that $\mathcal{M}_z=M_z\otimes (k_z\mapsto -k_z)$. However, since we are dealing with an ideal 2D model, the distinction will not be important until we consider a general 3D model (see Appendix D).

⁶It should be mentioned that even in the absence of mirror symmetry \mathcal{M}_z , the antiunitary symmetry \mathcal{TP} is sufficient to show that energy levels are doubly degenerate (and thus there are only three Fermi surfaces). The potential benefit of this extra condition is to obtain a canonical decoupling which will persist into the SC state when TRS is broken.

⁷The prime in $|\pm'\rangle$ is to denote a possible different vector (within the same \pm sector) than $|\pm\rangle$, e.g., $\langle x \uparrow | \varepsilon | z \downarrow \rangle$.

 $^{{}^8}S$, D, D' are capitalized to emphasize that the symmetries are only with respect to \mathbf{k} space and not orbitals and spin. It should be noted that the symmetries of each component were obtained assuming that the normal state $\varepsilon(\mathbf{k})$ is invariant under the point group D_{4h} . If, for example, 100 or 110 strain was included, the point group would shrink (though the normal state would still preserve mirror symmetry \mathcal{M}_z).

⁹Even in the absence of mirror symmetry \mathcal{M}_z , the symmetries $\mathcal{TP}, \mathcal{CP}$ are sufficient to show that every nonzero eigenenergy is doubly degenerate, while the zero eigenenergy space is quartic

degenerate. However, the mirror symmetry \mathcal{M}_z will make it possible to analyze nodal points of TRS breaking accidentally degenerate states, e.g., d + ig pairings.

¹⁰Due to the symmetry between $\hat{\Delta}_{\pm}$, we will drop the + subscript when referring to the gap matrix $\hat{\Delta}_{+}$.

TABLE II. **k**-space symmetry of components in gap matrix $\hat{\Delta}(\mathbf{k})$ in Eq. (3). The top row denotes the overall symmetry of the SC gap, while each entry denotes the k-space symmetry of the corresponding component, capitalized (S, D, D', G) to emphasize k-space symmetry only. The first four components (last five) correspond to singlet (triplet) pairing.

Component $C \setminus Symmetry$	S	d	d'	g
Δ_z	S	D	D'	\overline{G}
$\Delta_x + \Delta_y$	S	D	D'	G
$\Delta_x - \Delta_y$	D	S	G	D'
$\Delta_{x,y} + \Delta_{y,x}$	D'	G	S	D
$\Delta_{x,y} - \Delta_{y,x}$	S	D	D'	G
$\Delta_{x,z} + \Delta_{z,x} + i(\Delta_{y,z} - \Delta_{z,y})$	S	D	D'	G
$\Delta_{x,z} + \Delta_{z,x} - i(\Delta_{y,z} - \Delta_{z,y})$	D	S	G	D'
$\Delta_{y,z} + \Delta_{z,y} + i(\Delta_{x,z} - \Delta_{z,x})$	D'	G	S	D
$\Delta_{y,z} + \Delta_{z,y} - i(\Delta_{x,z} - \Delta_{z,x})$	G	D'	D	S

shadowed triplet in [26]), where

$$\hat{\Delta}^{\text{singlet}}(\mathbf{k}) = \begin{bmatrix} [c]\Delta_{x} & \Delta_{h} & 0\\ \Delta_{h} & \Delta_{y} & 0\\ 0 & 0 & \Delta_{z} \end{bmatrix}, \tag{4}$$

$$\hat{\Delta}^{\text{triplet}}(\mathbf{k}) = \begin{bmatrix} 0 & i\Delta_{h'} & \Delta_{x,z}\\ -i\Delta_{h'} & 0 & \Delta_{y,z}\\ \Delta_{z,x} & \Delta_{z,y} & 0 \end{bmatrix}, \tag{5}$$

$$\hat{\Delta}^{\text{triplet}}(\mathbf{k}) = \begin{bmatrix} 0 & i\Delta_{h'} & \Delta_{x,z} \\ -i\Delta_{h'} & 0 & \Delta_{y,z} \\ \Delta_{z,x} & \Delta_{z,y} & 0 \end{bmatrix}, \tag{5}$$

$$\Delta_h = \frac{1}{2} (\Delta_{x,y} + \Delta_{y,x}),\tag{6}$$

$$\Delta_{h'} = \frac{1}{2i} (\Delta_{x,y} - \Delta_{y,x}). \tag{7}$$

We emphasize that we do not assume SOC is weak; rather, the dominant singlet behavior is a phenomenological assumption. In this case, since G waves require unnaturally long-range interactions to generate, Table II implies that the g wave "naturally" lives mainly on the x, y bands, while all other one-dimensional (1D) irreps s, d, d' wave should have comparable magnitudes on all three bands. More specifically, a g wave can be generated via the form $\Delta_{x/y}(\mathbf{k}) = \pm D'(\mathbf{k})$ which only requires second-nearest-neighbor interactions. 11

E. Nodal structure

We now turn to the nodal structure of the dominantly singlet d + ig phase. In a multiband model, the nodal points are determined in a nonlinear manner by the SC gap Δ [i.e., by solving det $H(\mathbf{k}) = 0$] and thus the nodal structure of accidentally degenerate states does not follow trivially from analyzing 1D irreps individually, e.g., [17,19]. Typically, the stability of point nodes in 2D or line nodes in 3D is established under only under the assumption of unbroken TRS \mathcal{T} [35–38].

Below, we show that for the singlet d + ig pairing in a 2D system, the existence and stability [39] of point nodes along the (110), $(1\bar{1}0)$ directions can be established, despite the breaking of TRS, on the basis of unbroken \mathcal{M}_z (along with the usual \mathcal{M}_{xv}). A small admixture of subdominant triplet pairing due to SOC does not affect this result (see Appendix D). In a general 3D model, however, this argument only applies in the $k_z = 0$, π planes; for all other (nonmirror invariant) values of k_z , the line nodes of the 2D problem expand into narrow surfaces of gapless Bogoliubov quasiparticles (similar to [40]), that become "pinched" into points at the $k_z = 0$ and π planes. The radius of these "Bogoliubov Fermi surfaces" is small in proportion to the coupling of eigenspaces $\mathcal{M}_z=\pm i$ (see Appendix D).

In the Sr₂RuO₄ context, any such Bogoliubov Fermi surfaces would be small both as a consequence of the smallness of the spin-conserving hybridization between the x, z and y, zbands¹³ and atypical forms of SOC¹⁴ in units of the bandwidth. Thus, a multiband d + ig phase will display properties characteristic of vertical line nodes (such as a linear dependence of the density of states in energy) down to extremely low energies, consistent with the nodal behavior of the singleband d + ig phase.

1. Existence of line nodes

By symmetry considerations tabulated in Table II, if the overall symmetry is of singlet d + ig pairing, then along the (110), $(1\bar{1}0)$ directions, the only nonzero component of the gap matrix $\hat{\Delta}(\mathbf{k})$ is $\Delta_x(\mathbf{k}) - \Delta_y(\mathbf{k})$ [which we refer to as $2\Delta_3(\mathbf{k})$ and possibly a complex number, i.e., $\Delta_3(\mathbf{k}) \equiv$ $e^{i2\theta(\mathbf{k})}|\Delta_3(\mathbf{k})|$]. It is then clear that by performing a **k**conserving gauge transform, the quasiparticle Hamiltonian $H_{+}(\mathbf{k})$ with complex $\Delta_{3}(\mathbf{k})$ is mapped unitarily to that with non-negative $|\Delta_3(\mathbf{k})|$, i.e.,

$$e^{-i\theta\tau_3}H_+(\hat{\varepsilon}_+, \Delta_3)e^{i\theta\tau_3} = H_+(\hat{\varepsilon}_+, |\Delta_3|), \tag{8}$$

where τ_3 denotes the Pauli matrix in particle-hole space and H_{+} depends on **k** implicitly via $\hat{\varepsilon}(\mathbf{k})$, $\Delta_{3}(\mathbf{k})$. Equivalently, the gauge transform maps the TRS breaking k-conserving Hamiltonian $H_{+}(\mathbf{k})$ to such that preserves TRS, ¹⁵ and thus a line node can be found explicitly along the (110), $(1\bar{1}0)$ directions (see Appendix C). It is worth mentioning that if we consider a triplet d + ig pairing, by Table I or II, there are two nonzero components along the (110), (1 $\bar{1}$ 0) directions and thus the argument breaks down.

¹¹Indeed, a state with $\Delta_{x,y} = \Delta_{y,x} = D$ has g-wave symmetry involving only nearest-neighbor pairing. However, since the hybridization ε_h in the band structure is generally small compared to the diagonal terms ε_x , ε_y , ε_z , the off-diagonal components of the gap matrix $\hat{\Delta}$ are typically small for reasons unrelated to their range.

¹²A similar proof can be adapted to show the existence and stability of line nodes along the (100), (010) directions for d' + ig pairing.

¹³Terms of the form $\langle xs|\varepsilon(\mathbf{k})|zs\rangle$, $\langle ys|\varepsilon(\mathbf{k})|zs\rangle$ for $s=\uparrow,\downarrow$, which break the action of mirror symmetry \mathcal{M}_z on the orbital and spin space (couple the $|\pm\rangle$ bases).

¹⁴Terms such as $\langle x \uparrow | \varepsilon(\mathbf{k}) | x \downarrow \rangle$, $\langle x \uparrow | \varepsilon(\mathbf{k}) | y \downarrow \rangle$, since the typical form $\varepsilon_{\text{SOC}}(\mathbf{k})\mathbf{l}\cdot\boldsymbol{\sigma}$ in Eq. (1) preserves SU(2) action on the orbital and spin space and, thus, even for $k_z \neq 0$, π , is decoupled in the orbital and spin bases $|\pm\rangle$.

¹⁵Indeed, gauge symmetry is the reason why single-band d + igstates can still have stable line nodes despite breaking TRS.

TABLE III. First three harmonics ($R \le 2$) based on symmetry and normalized via their squared integral. The 0 implies that there does not exist such a symmetry component for the given range. We have omitted the $G_R(\mathbf{k})$ wave since it does not appear until fourth-nearest-neighbor interactions (R = 4).

Lattice	Harmonic	R = 0	R = 1	R=2
(A_{1g})	$S_R(\mathbf{k})$	1	$\cos k_x + \cos k_y$	$2\cos k_x\cos k_y$
(B_{1g})	$D_R(\mathbf{k})$	0	$\cos k_x - \cos k_y$	0
(B_{2g})	$D_R'(\mathbf{k})$	0	0	$2 \sin k_x \sin k_y$

III. NUMERICAL RESULTS

A. Setup

Since on physical grounds, we plan to deal only with the case in which the effective interactions are short ranged, it is convenient to introduce *lattice harmonics*, specified by their range R and their symmetry, which form an ordered basis for any lattice function. The first few such harmonics for each relevant symmetry are shown in Table III, normalized via their squared integral (L^2 norm). Thus, for example, we can decompose a D wave in \mathbf{k} space into a linear combination of lattice harmonics $D_R(\mathbf{k})$ of range R (where R=0 indicates onsite, R=1 is nearest neighbors, R=2 is next-nearest neighbors, etc.).

We can then consider an effective interaction in the BCS channel of the form

$$\mathcal{V} = \frac{1}{2} \sum_{\mu \mu', \mathbf{k} \mathbf{k}'} V_{\mu \mu'}(\mathbf{k} - \mathbf{k}') P_{\mu}^{\dagger}(\mathbf{k}) P_{\mu'}(\mathbf{k}'), \tag{9}$$

where $P_{\mu}(\mathbf{k}) = \psi_{\downarrow\mu}(-\mathbf{k})\psi_{\uparrow\mu}(\mathbf{k})$ annihilates a Cooper pair in band μ and $V_{\mu\mu'}(\mathbf{q})$ represents the interaction between bands μ , μ' . By construction, the form of $V_{\mu\mu'}(\mathbf{q})$ precludes interband pairing of the SC gap, i.e., the self-consistency equations imply $\Delta_h = 0$; a more general form of the interaction would generally lead to a small but nonzero Δ_h , but this would not change any of our findings qualitatively.

We shall take interactions that respect the lattice symmetries and have range $R \leq 2^{16}$:

$$V_{\mu\mu'}(\mathbf{q}) = \sum_{R=0,1,2} v_{\mu\mu'}(R) S_R(\mathbf{q}), \tag{10}$$

where S_R is given by the first row in Table III. It is then convenient to express V as a sum of terms of the form $c_a\psi_a(\mathbf{k})\psi_a(\mathbf{k}')$ where each $\psi_a(\mathbf{k})$ transforms according to one of the irreps (S, D, D') of the point group and decomposed into harmonics tabulated in Table III. We leave the details of the decomposition in Appendix E. For completeness, the nonlinear gap equation is given here

$$\Delta_{\mu}(\mathbf{k}) = \sum_{\mu'\mathbf{k}'} V_{\mu\mu'}(\mathbf{k} - \mathbf{k}') \langle P_{\mu'}(\mathbf{k}') \rangle, \tag{11}$$

¹⁶By symmetry, it is possible that $V_{x,x}(\mathbf{q}) \neq V_{y,y}(\mathbf{q})$ and $V_{x,z}(\mathbf{q}) \neq V_{y,z}(\mathbf{q})$. However, the differences $(V_{x,x} - V_{y,y})(\mathbf{q})$ and $(V_{x,z} - V_{y,z})(\mathbf{q})$ must satisfy B_{1g} symmetry with respect to \mathbf{q} . Therefore, for each tion range $R \leq 2$, the interactions can only mix s and $d_{x^2-y^2}$ wave harmonics, e.g., $(V_{x,x} - V_{y,y})(\mathbf{k} - \mathbf{k}') = s_1(\mathbf{k})d_1(\mathbf{k}') + d_1(\mathbf{k})s_1(\mathbf{k}') + \cdots$, and thus have no direct effect on the R = 2 harmonics involving the d_{xy} or g waves.

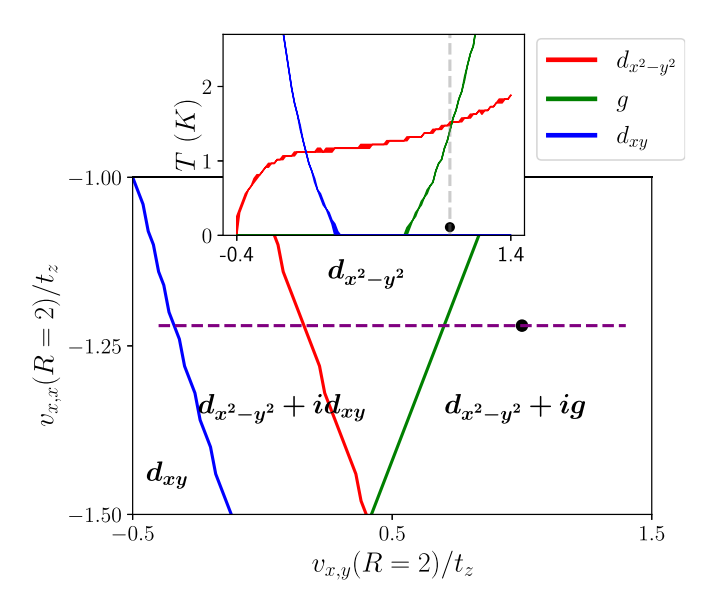


FIG. 2. The T=0 phase diagram in a representative 2D plane in the multidimensional parameter space of interactions. The black point corresponds to a point at which d and g are degenerate, with parameters listed in Table IV; we will use these parameters in later analysis including those reported in Figs. 3 and 4. In the main figure, all interactions with range R<2 are held fixed, while those with R=2 are varied maintaining the (arbitrarily chosen) relation $v_{z,z}=0.73v_{x,y}-0.43$, where the slope is positive so that $v_{z,z}, v_{x,y}$ do not compete [41]. The inset represents the thermal phase diagram along the 1D cut through parameter space indicated by the dashed line in the main figure. The different color solid lines are phase boundaries corresponding to the point at which the indicated symmetry order parameters vanish.

where the expectation value $\langle \dots \rangle$ is taken with respect to the BCS Hamiltonian.

For simplicity, we will henceforth set SOC to zero since it does not qualitatively affect the results. In particular, the Lifshitz transition occurs at \mathbf{k} points $(\pi,0)$, $(0,\pi)$, where the orbital character of each band is well defined and thus the SOC terms are weak in any case. In this limit, the two-band system consisting of the α and β bands decouples from the γ band within the BCS Hamiltonian, though all three bands are still coupled via the interaction term $\mathcal V$ in the nonlinear gap equation in Eq. (11). Using the fact that SU(4) is the spin group of SO(6), we provide an intuitive manner of diagonalizing the 4×4 BdG Hamiltonian involving the two-band system, details of which are left in Appendix F.

B. Zero temperature T=0

Figure 2 shows a cut through the T=0 phase diagram in response to intraband and interband couplings, obtained by solving the self-consistent BCS equations described in Eq. (11). Indeed, as previously argued, by Tables II and III, a g-wave SC gap with range $R\leqslant 2$ must satisfy $\Delta_z=\Delta_x+\Delta_y=0$ and thus must be constructed via the anticipated form $\Delta_{x/y}(\mathbf{k})=\pm D'(\mathbf{k})$. Moreover, since $D'_R(\mathbf{k})$ is first nonzero for second neighbor R=2, the range R=2 interactions (including both intraband $v_{x,x}, v_{z,z}$ and interband $v_{x,y}$) are responsible for generating d_{xy} - or g-wave symmetries. The remaining in-

TABLE IV. Specific parameters (in units of the nearest-neighbor hopping t_z on the γ band) chosen of the interaction term in Eq. (10) corresponding to the dot in Fig. 2. Note that in Fig. 2, only $v_{x,x}(2)$, $v_{x,y}(2)$ were varied.

Interaction v/t_z	R = 0	R = 1	R=2
$\overline{v_{z,z}(R)}$	7	-0.4	0.3
$v_{x,x}(R)$	5	-0.1	-1.2
$v_{x,y}(R)$	5	-0.1	1
$v_{x,z}(R)$	5	0.1	0.1

teraction parameters are fixed and given in Table IV, tuned so that at T=0 there exists a background $d_{x^2-y^2}$ wave. Throughout, the preferred phase relation between the two components is such as to break time-reversal symmetry, i.e., $d_{x^2-y^2} \pm ig$ or $d_{x^2-y^2} \pm id_{xy}$.

In the vast parameter space of interactions, it is probably unsurprising that we can find regions in which the $d_{x^2-y^2}$ and g waves coexist. However, while in any single-band problem, such coexistence regions are generically exceedingly narrow, here the coexistence region is relatively large, reflecting the fact that the two components live primarily on different bands, and so hardly compete with one another. Within the coexistence regions, the transition temperatures of the two orders are comparable, i.e., $T_c \sim T_{\text{TRSB}}$. Indeed, in the inset graph in Fig. 2, we plot the onset temperature T_{onset} of each component $(d_{x^2-y^2}, g, d_{xy})$ waves) along the given cut (dashed purple line) in the phase diagram. As the secondary order component transitions from $d_{xy} \rightarrow g$ wave (left to right), the corresponding background $d_{x^2-y^2}$ wave has an increase in T_c .

C. Splitting of T_c , T_{TRSB} with uniaxial stress

Let us tune the parameters to the dot in Fig. 2 so that the ground state has $d_{x^2-y^2}\pm ig$ pairing and $T_c\approx T_{\rm TRSB}$ in the absence of strain. We model the effect of uniaxial stress (parametrized by ε_{xx}) by varying the band parameters in a manner consistent with experiment [12,32] such that the γ band crosses the Van Hove point $(0,\pm\pi)$ at $\varepsilon_{xx}\approx -0.44\%$ (details in Appendix G). The α , β bands are also distorted, but only slightly [32].

The resulting critical temperature for the d and g components are given in Fig. 3. Due to symmetry-breaking uniaxial stress, the point-group symmetry D_{4h} is broken, while the subgroup D_{2h} is preserved. This implies that the $d_{x^2-y^2}$ component in general gains an s-wave component. Similarly, the g wave should also gain a d_{xy} -wave component. However, our

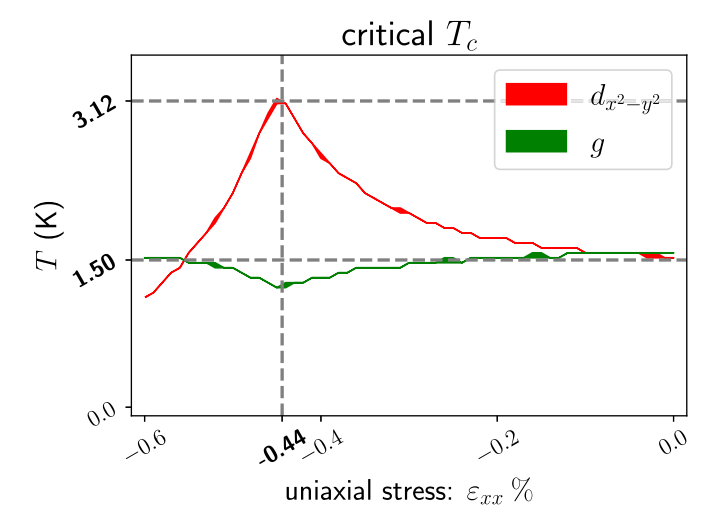


FIG. 3. Critical temperatures. The red and green lines represent the critical temperatures of the d- and g-wave components. (The thickness denotes numerical uncertainty in the result based on calculations on a 3000^2 -site square lattice.) The Lifshitz transition occurs at a uniaxial stress $\varepsilon_{xx} \approx -0.44\%$.

numerical calculations show that the additional d_{xy} is much smaller than the g-wave component. This is presumably due to the fact that the α , β bands are minimally distorted in the presence of strain, while the strong d- or (d+s)-wave component on the γ band suppresses any other symmetry component. Therefore, we label the corresponding symmetries as given in the legend of Fig. 3.

In the presence of small uniaxial stress $\varepsilon_{xx} \gtrsim -0.2\%$, away from the Lifshitz transition, the critical temperatures remain remarkably close to each other, and thus the accidentally degenerate d+ig state is stable when the DOS remains roughly constant. Near the Van Hove point $\varepsilon_{xx} \approx -0.44\%$, the d-wave channel is enhanced causing the observed split in $T_c > T_{\text{TRSB}}$. At a value of the strain somewhat beyond the Van Hove point, $\varepsilon_{xx} \lesssim -0.5\%$, our calculations suggest that the g-wave component is first observed when entering superconductivity. However, note that in the context of short-range ordere (SRO), there exists an observed competing spin-density-wave (SDW) [29] which is not incorporated in our calculations.

D. Response to pure B_2 and A_1 strain

We again tune the parameters to the dot in Fig. 2 so that the d, g waves are accidentally degenerate and investigate the response of our multiband model to pure B_2 and pure A_1 strain. The resulting critical temperatures regarding the onset of d and g waves are shown in Fig. 4. In Fig. 4(a), symmetry-breaking B_2 strain is simulated by modifying the second-nearest-neighbor (R = 2) hoppings in the normal-state band structure (details in Appendix G). In this case, the critical temperatures remain remarkably close to each other even at large strain values (at which the relative phase between the d, g components is $\theta = 0$) and thus provides further evidence to the stability of the accidental degeneracy in the presence of strain. In Fig. 4(b), we introduced pure A_1 strain by tuning the relative energies of the three bands so that the γ band is driven towards (away from) the Van Hove singularity for negative (positive) values ε , with the total density of electrons held

¹⁷Along the *x* axis of Fig. 2, the presence of a d_{xy} wave would imply comparable magnitude on all three bands and thus induces strong competition with the $d_{x^2-y^2}$ wave. Therefore, the accidental degeneracy between the $d_{x^2-y^2}$ and d_{xy} states is quickly destroyed by the preference for a pure d_{xy} wave as shown in inset of Fig. 2. In contrast, the *g*-wave component mainly lives on the *α*, *β* bands by symmetry requirements and thus there is a natural ground state where the background $d_{x^2-y^2}$ shifts progressively to the *γ* band to minimize competition. A similar logic would apply in the instance where the background state is an *s* wave instead of a $d_{x^2-y^2}$ wave.

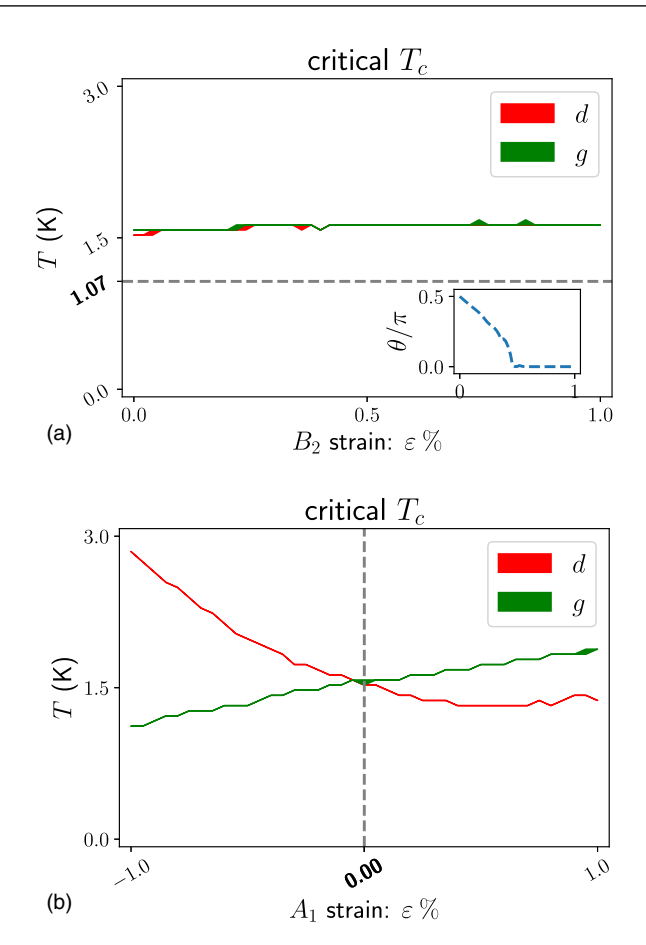


FIG. 4. The red and green lines represent the critical temperature T at which the d and g waves occur under (a) pure B_2 strain and (b) pure A_1 strain. The inset in subplot (a) shows the relative phase between the d and g waves near T_c , i.e., along the horizontal dashed line in (a).

fixed (see Appendix G). This results in a crossover between the d, g waves, i.e., for $\varepsilon < 0$ the d wave is favored over the g wave and vice versa, resulting in a kinklike feature in the overall T_c [maximum of the two lines in Fig. 4(b)] at $\varepsilon = 0$. No such kink has been detected in experiments on SRO to date [34].

IV. SUMMARY

Although Sr₂RuO₄ would seem to be the ideal material to serve as the model system for unconventional superconductivity, given that its normal state is an extremely well-characterized Fermi liquid, even the symmetries of the superconducting state have remained controversial [5]. Ultimately, this issue can only be settled by either reproducible phase-sensitive measurements, or by direct imaging (e.g., by angle-resolved photoemission or quasiparticle interference) of the gap structure on the Fermi surfaces. However, in the absence of these, further progress must rely on more indirect evidence based on comparisons between relatively robust aspects of theory and experimentally detected trends. Some of these aspects depend only on symmetry. However, while microscopic aspects of the problem are more difficult to access unambiguously, certain features, especially those that relate

directly to qualitative aspects of the known band structure, can be useful for the present purposes.

Here, we have analyzed a simple microscopic model with the band structure of Sr_2RuO_4 and effective pairing interactions treated as phenomenological input (we make no claims to the origin of the effective interaction). We have found several features of the solution of this problem that lend credence to the conjecture that the peculiar difficulty in settling the order-parameter question arises from an accidental near degeneracy between a $d_{x^2-y^2}$ -wave and g-wave pairing tendency. Specifically, we find the following suggestive results:

- (i) It is sufficient to consider a model with relatively short-ranged pairing effective interactions, out to second-neighbor distance. In common with many previous studies [42–45], we find that the generic result is that pairing is dominant either on the γ band or on the α and β bands. Thus, in any case, a certain degree of fine tuning of the interactions is necessary to ensure that the gap magnitude is comparable on all bands (as is experimentally established [46]).
- (ii) Under circumstances of near degeneracy, the $d_{x^2-y^2}$ -wave pairing occurs dominantly on the γ band and the g wave on the α and β bands. Loosely, this near degeneracy requires no more fine tuning than is required to have comparable gaps on all bands.
- (iii) As a consequence, if the band structure is tuned (for instance by uniaxial stress) such that the γ band approaches the nearby Van Hove point, this can significantly enhance the d-wave component of the order parameter, but has relatively little effect on the g wave. (Generally, if two components coexist in the same bands, then whatever enhances one tends to suppress the other.)
- (iv) The existence of gapless (nodal) quasiparticles is protected by symmetry, even if time-reversal symmetry is broken in a dominantly singlet $d_{x^2-y^2}+ig$ state, so long as the mirror symmetry \mathcal{M}_z (along with the usual \mathcal{M}_{xy}) of the crystal is unbroken. Conversely, similar to the single-band model, \mathcal{M}_{xy} breaking strain can induce a SC gap which can be detected in experiment.

While none of these results are sufficiently unique to serve as confirmation of the basic scenario, they serve to increase confidence in its "naturalness."

Note added. Recently, in Ref. [47] the authors stabilized a $d_{x^2-y^2}+ig$ state via introducing a second-nearest-neighbor term in the bare interaction. Although the calculation was done in the weak coupling limit in terms of random phase approximation (RPA), it agrees with our proposal that a relatively short-ranged model is sufficient to stabilize a g-wave component. In contrast, Ref. [24] proposes a multipole-fluctuation pairing mechanism to stabilize a $d_{x^2-y^2}+ig$ state. In doing so, they assumed a long-range interaction $(\sim 1/q^2)$ in momentum space) which may have been the reason for stabilizing a secondary g-wave symmetry.

ACKNOWLEDGMENTS

S.A.K. and A.Y. were supported, in part, by NSF Grant No. DMR-2000987 at Stanford. E.B. was supported by the European Research Council (ERC) under grant HQMAT (Grant Agreement No. 817799), the Israel-US Binational Science

Foundation (BSF), and a Research grant from Irving and Cherna Moskowitz.

APPENDIX A: BAND STRUCTURE

The normal-state dispersion values used in this paper are found in the Supplemental Material (SM) of Ref. [49]. We repeat them here for completeness, i.e.,

$$\varepsilon_{x/y}(\mathbf{k}) = -\mu_0 - 2t_x \cos k_{x/y} - 2t_y \cos k_{y/x}, \tag{A1}$$

$$\varepsilon_z(\mathbf{k}) = -\mu_z - 2t_z(\cos k_x + \cos k_y) - 2t_z'(2\cos k_x \cos k_y),$$
(A2)

$$\varepsilon_h(\mathbf{k}) = 4t_h \sin k_x \sin k_y,\tag{A3}$$

where for Sr_2RuO_4 , we use the values, the SO coupling was taken to be $\varepsilon_{SOC} = 30$ meV.

$t_z (\text{meV})$	$t_x \text{ (meV)}$	t_y/t_x	t_h/t_x	μ_z/t_z	μ_x/t_x
119	165	0.08	0.13	1.48	1.08

APPENDIX B: SYMMETRY OPERATORS

We shall briefly discuss the explicit forms and properties of symmetry operators, i.e., particle-hole symmetry (PHS) \mathcal{C} , time-reversal symmetry (TRS) \mathcal{T} , and generators of the point group D_{4h} , i.e., parity \mathcal{P} , mirror symmetries \mathcal{M}_z , \mathcal{M}_{xy} , and $\pi/2$ -rotation symmetry \mathcal{C}_4 . Notice that, except for PHS \mathcal{C} , all other symmetries discussed will be restricted to the particle space. Their extension to particle-hole space follows uniquely that they commute with PHS \mathcal{C} . More specifically, $\langle a_h|\mathcal{O}|b_h\rangle = \langle a_p|\mathcal{O}^*|b_p\rangle$ where \mathcal{O}^* denotes complex conjugation of symmetry operator \mathcal{O} and the subscripts h, p denote hole, particle states:

- (1) PHS C is an antiunitary map on particle-hole space, which takes particle state to hole state and vice versa, and maps the wave vector $\mathbf{k} \mapsto -\mathbf{k}$. In particular, $C^2 = 1$.
- (2) TRS \mathcal{T} is regarded as antiunitary map on particle space, which acts as $\exp(-i\pi\sigma_2/2)$ on spin space, acts trivially on orbital space, and maps the wave vector $\mathbf{k} \mapsto -\mathbf{k}$. In particular, TRS reverse the spin operators, i.e., $\mathcal{T}\sigma_i\mathcal{T}^{\dagger} = -\sigma_i$ where σ_i are the Pauli matrices acting on spin space.
- (3) Parity \mathcal{P} is consistent with its real-space transform $x, y, z \mapsto -x, -y, z$. Hence, it acts trivially on spin and orbital space, and maps $\mathbf{k} \mapsto -\mathbf{k}$.
- (4) Mirror symmetry \mathcal{M}_z is consistent with its real-space transform $x, y, z \mapsto x, y, -z$. More specifically, it acts as $\exp(-i\pi\sigma_3/2)$ on spin space [an SU(2) action which canonically maps to $\mathcal{PM}_z \in SO(3)$], maps $d_{yz}, d_{zx}, d_{xy} \mapsto -d_{yz}, -d_{zx}, +d_{xy}$ orbitals, and maps the wave vector $\mathbf{k} \mapsto \mathcal{M}_z^{-1}\mathbf{k} \equiv (k_x, k_y, -k_z)$. Due to spin space, $\mathcal{M}_z^2 = -1$.
- (5) Mirror symmetry \mathcal{M}_{xy} is consistent with its real-space transform $x, y, z \mapsto y, x, z$. More specifically, it acts as $\exp[-i\pi(\hat{n}\cdot\sigma)/2]$ on spin space where \hat{n} is the unit vector in (-1, 1, 0) direction [an SU(2) action which canonically maps to $\mathcal{P}\mathcal{M}_{xy} \in SO(3)$], maps $d_{yz}, d_{zx}, d_{xy} \mapsto d_{zx}, d_{yz}, d_{xy}$ orbitals, and maps the wave vector $\mathbf{k} \mapsto \mathcal{M}_{xy}^{-1} \mathbf{k} \equiv (k_y, k_x, k_z)$. Due to spin space, $\mathcal{M}_{xy}^2 = -1$.

TABLE V. Mapping of group operations $\mathcal{O} = \mathcal{C}_4$, \mathcal{M}_{xy} of D_{4h} where $\mathbf{k}' \equiv \mathcal{O}^{-1}\mathbf{k}$.

Operation g	Mapping		
	$\varepsilon_z(\mathbf{k}) \mapsto \varepsilon_z(\mathbf{k}')$		
C	$(\varepsilon_x \pm \varepsilon_y)(\mathbf{k}) \mapsto \pm (\varepsilon_x \pm \varepsilon_y)(\mathbf{k}')$		
$\mathcal{M}_{x,y}$	$\varepsilon_h(\mathbf{k}) \mapsto -\varepsilon_h(\mathbf{k}')$		
	$arepsilon_{ ext{SOC}}(\mathbf{k}) \mapsto arepsilon_{ ext{SOC}}(\mathbf{k}')$ $arepsilon_z(\mathbf{k}) \mapsto arepsilon_z(\mathbf{k}')$		
	$(\varepsilon_x \pm \varepsilon_y)(\mathbf{k}) \mapsto \pm (\varepsilon_x \pm \varepsilon_y)(\mathbf{k}')$		
	$\varepsilon_h(\mathbf{k}) \mapsto +\varepsilon_h(\mathbf{k}')$		
	$\varepsilon_{\mathrm{SOC}}(\mathbf{k}) \mapsto \varepsilon_{\mathrm{SOC}}(\mathbf{k}')$		

(6) $\pi/2$ rotation \mathcal{C}_4 is consistent with its real-space transform $x, y, z \mapsto y, -x, z$. More specifically, it acts as $\exp(-i\pi\sigma_3/4)$ on spin space [an SU(2) action which canonically maps to $\mathcal{C}_4 \in \mathrm{SO}(3)$], maps $d_{yz}, d_{zx}, d_{xy} \mapsto -d_{zx}, d_{yz}, -d_{xy}$ orbitals, and maps the wave vector $\mathbf{k} \mapsto \mathcal{C}_4^{-1}\mathbf{k} \equiv (-k_y, k_x, k_z)$.

Notice that within certain planes (e.g., $k_z = 0$, π plane for \mathcal{M}_z and $k_x = k_y$ plane for \mathcal{M}_{xy}), the mirror symmetries \mathcal{M}_z , \mathcal{M}_{xy} are local in **k** and thus only act nontrivially in the orbital and spin space. Therefore, it is useful to define M_z , M_{xy} as their orbital and spin actions so that $\mathcal{M}_z = M_z \otimes (k_z \mapsto -k_z)$ and $\mathcal{M}_{xy} = M_{xy} \otimes (k_x \leftrightarrow k_y)$.

Normal-state symmetries

Using the explicit forms of point-group symmetries of D_{4h} discussed in the previous section, one finds that the matrix components of the normal-state dispersion are mapped in a rather complicated manner and thus tabulated in Table V. Since the normal state is invariant under the point group D_{4h} , it is then clear that $\varepsilon_x + \varepsilon_y$, $\varepsilon_x - \varepsilon_y$, ε_h satisfy (S, D, D')-wave (A_{1g}, B_{1g}, B_{2g}) symmetry in **k** space, respectively. Compare this to the specific parametrization in Appendix A. A similar analysis can be done for the SC state with regards to the SC gap $\Delta(\mathbf{k})$.

APPENDIX C: EXISTENCE OF LINE NODE

Continuing the argument from Sec. II E 1, notice that $H_+(\hat{\varepsilon}, |\Delta_3|)$ can be decomposed into $= \tau_1 \lambda_3 |\Delta_3| + \tau_3 \hat{\varepsilon}_+$ [where $\lambda_3 = \text{diag}(1, -1, 0)$ is the third Gell-Mann matrix] and thus anticommutes with τ_2 . Hence, the determinant (which is invariant under unitary transforms) is given by

$$\det H_{+}(\mathbf{k}) = |\det[\hat{\varepsilon}_{+}(\mathbf{k}) + i|\Delta_{3}(\mathbf{k})|\lambda_{3}]|^{2}, \quad (C1)$$

where **k** is restricted along the (110), (1 $\bar{1}$ 0) directions. Therefore, there exists a nodal point if and only if $\det(\hat{\varepsilon}_+ + i|\zeta|\lambda_3) = 0$. Notice that mirror symmetry \mathcal{M}_{xy} maps $\lambda_3 \mapsto -\lambda_3$ while keeping $\hat{\varepsilon}_+$ invariant. Therefore, $\det(\hat{\varepsilon}_+ + i|\Delta_3|\lambda_3) = \det(\hat{\varepsilon}_+ - i|\Delta_3|\lambda_3)$ is a real value along the (110), (1 $\bar{1}$ 0) directions. The nodal equation $\det(\hat{\varepsilon}_+ + i|\Delta_3|\lambda_3) = 0$ thus corresponds to one real equation (instead of 2 where both the real and imaginary components are required

to be zero), and thus defines a line node along the (110), ($1\bar{1}0$) directions.

For completeness, the nodal equation can be computed explicitly to be

$$|\Delta_3(\mathbf{k})|^2 \varepsilon_7(\mathbf{k}) + \det \hat{\varepsilon}(\mathbf{k}) = 0$$
 (C2)

and in the absence of SOC, $\varepsilon_{\rm SOC}=0,$ the equation reduces to

$$|\Delta_3(\mathbf{k})|^2 = \varepsilon_h(\mathbf{k})^2 - \varepsilon_x(\mathbf{k})^2. \tag{C3}$$

Since the gap function is usually the smallest scale in the system, the equation generally holds true at some point along the diagonals, near the intersection of the FS of the x, y bands, despite the fact that $\Delta_3 \neq 0$.¹⁸

APPENDIX D: RIGOROUS PERTURBATIVE ARGUMENT

1. Setup

Let us consider a general 3D multiband $d_{x^2-y^2} + ig$ state $H(\mathbf{k})$ with spin degree of freedom so that $H(\mathbf{k})$ is a $4n \times 4n$ matrix at each wave vector \mathbf{k} (n=3 is the number of orbitals in $\mathrm{Sr_2RuO_4}$). We shall assume that $H(\mathbf{k})$ has arbitrarily strong SOC and dominantly singlet with possible subdominant triplet pairing and weak k_z dependence so that we can treat the triplet pairing and k_z dependence perturbatively. Let $H^s(\mathbf{k})$ be obtained from $H(\mathbf{k})$ by setting the triplet-pairing gap elements =0, i.e., the purely singlet portion so that in particle-hole space,

$$H(\mathbf{k}) = H^{s}(\mathbf{k}) + \begin{bmatrix} 0 & \Delta^{\text{triplet}}(\mathbf{k}) \\ \Delta^{\text{triplet}}(\mathbf{k})^{\dagger} & 0 \end{bmatrix}.$$
 (D1)

Let us further define

Here define
$$H_0^{\rm s}(\mathbf{k}) = \sum_{m=\pm i} 1_{M_z=m} H^{\rm s}(\mathbf{k}) 1_{M_z=m},$$
 (D2)

$$H_0(\mathbf{k}) = \sum_{m=+i} 1_{M_z=m} H(\mathbf{k}) 1_{M_z=m},$$
 (D3)

where $1_{M_z=\pm i}$ are the projection operators onto the eigenspaces of the orbital and spin action $M_z=\pm i$. In this case, $H_0(\mathbf{k}), H_0^s$ are decoupled in the eigenspaces $M_z=\pm i$ which was the essential ingredient in our restricted 2D model in the main text. It is worth mentioning that, here, $H_0(\mathbf{k})$ and $H_0^s(\mathbf{k})$ may have k_z dependence.

Notice that mirror symmetry \mathcal{M}_{xy} maps $\Delta(\mathbf{k}) \mapsto -\Delta(\mathbf{k})$ so that after a gauge transform $\mathcal{U} = i\tau_3$ (where τ_3 is the Pauli matrix in particle-hole space), the Hamiltonian $H(\mathbf{k})$ is invariant $\mathcal{U}\mathcal{M}_{xy} \equiv \tilde{\mathcal{M}}_{xy}$. Subsequently, the restricted Hamiltonians H^s , H_0 , H_0^s are also invariant under $\tilde{\mathcal{M}}_{xy}$.

2. Starting point: Decoupled singlet Hamiltonian

As discussed in the main text, since $H_0^s(\mathbf{k})$ is of purely singlet pairing and is decoupled in the eigenspaces of $M_z = \pm i$, it has a line node extended in the k_z direction in the (110) direction, which we denote by $\mathbf{k}_0^s(k_z)$. Let us fix k_z , and thus from Theorem 1, it is clear that dim ker $H_0^s(\mathbf{k}_0^s) = 4m$ for some $m \ge 1$. In the absence of other symmetries, it is generally

assumed that m=1 so that we can choose $\phi_0^s(\mathbf{k}_0^s)$ so that $\{\phi_0^s(\mathbf{k}_0^s)\} = (\phi_0^s, \tilde{M}_{xy}\phi_0^s, \mathcal{CP}\phi_0^s, \mathcal{CP}\tilde{M}_{xy}\phi_0^s)$ forms a basis for $\ker H_0^s(\mathbf{k}_0^s)$, and we shall use $P_0^s(\mathbf{k}_0^s)$ to denote the projection operator onto $\ker H_0^s(\mathbf{k}_0^s)$.

3. Adding mirror-symmetric perturbations, e.g., weak triplet pairing

Let us fix k_z as before, and let \mathbf{k} be near $\mathbf{k}_0^s(k_z)$ along the (110) direction so that $\tilde{\mathcal{M}}_{xy} = \tilde{M}_{xy}$. Since triplet pairing is subdominant, we can assume that $H_0(\mathbf{k}) - H_0^s(\mathbf{k}_0^s)$ with respect to the gap of $H_0^s(\mathbf{k}_0^s)$ [lowest nonzero energy level of $H_0^s(\mathbf{k}_0^s)$ and not to be confused with the gap function $\Delta(\mathbf{k}_0^s)$] when \mathbf{k} is near \mathbf{k}_0^s so that $P_0(\mathbf{k})$ can be well defined as the projection operator onto eigenstates of $H_0(\mathbf{k})$ with energies near zero and also unitarily equivalent to $P_0^s(\mathbf{k}_0^s)$ as explained in Appendix D 6. By perturbation theory (Weyl's inequality), the variation of the energy values must be small and thus it is sufficient to consider the restriction of $H_0(\mathbf{k})$ to $P_0(\mathbf{k})$ when attempting find the zero energies of $H_0(\mathbf{k})$, i.e., only eigenstates in $P_0(\mathbf{k})$ have energies sufficiently close to zero.

Since $H_0(\mathbf{k})$ is decoupled in the eigenspaces of $M_z = \pm i$ and invariant under mirror symmetry \tilde{M}_{xy} , from Theorem 1, there must exist $\phi_0(\mathbf{k})$ such that $\{\phi_0(\mathbf{k})\}$ forms a complete orthonormal basis for $P_0(\mathbf{k})$ (though not necessarily degenerate anymore). As an analogy, $\phi_0(\mathbf{k})$, $\tilde{M}_{xy}\phi_0(\mathbf{k})$ should be considered as "pseudospins" in particle space, while the remaining states are considered as "pseudospins" in hole states. Within the basis $\{\phi_0(\mathbf{k})\}$, the restriction $H_0(\mathbf{k})P_0(\mathbf{k})$ must be of the form

$$H_0(\mathbf{k})P_0(\mathbf{k}) = \begin{bmatrix} \hat{\varepsilon}_0(\mathbf{k}) & \hat{\Delta}_0(\mathbf{k}) \\ \hat{\Delta}_0(\mathbf{k})^{\dagger} & -\hat{\varepsilon}_0(-\mathbf{k})^T \end{bmatrix}.$$
 (D4)

By \mathcal{CP} symmetry, $\hat{\Delta}_0(\mathbf{k})$ must form a singlet between the pseudospins, i.e., in the basis representation $\{\phi_0(\mathbf{k})\}$, the matrix $\hat{\Delta}_0(\mathbf{k}) = \Delta_0(\mathbf{k})(i\sigma_2)$ where $\Delta_0(\mathbf{k}) \in \mathbb{C}$ and σ denotes the Pauli matrix in pseudospin basis. Furthermore, under the basis $\{\phi_0(\mathbf{k})\}$, the symmetries M_z , \tilde{M}_{xy} have the matrix forms

$$M_{z} = \begin{bmatrix} +i & & & & & \\ & -i & & & & \\ & & -i & & & \\ & & & +i \end{bmatrix},$$

$$\tilde{M}_{xy} = \begin{bmatrix} & +1 & & & \\ +1 & & & & \\ & & +1 & & \\ & & & +1 \end{bmatrix}.$$
 (D5)

Since $H_0(\mathbf{k})P_0(\mathbf{k})$ preserves the local symmetries M_z , \tilde{M}_{xy} , explicit calculations show that $\hat{\varepsilon}_0(\mathbf{k}) = \varepsilon_0(\mathbf{k})\sigma_0$ where $\varepsilon_0(\mathbf{k}) \in \mathbb{R}$ and $\hat{\Delta}_0(\mathbf{k}) = 0$. Therefore,

$$H_0(\mathbf{k})P_0(\mathbf{k}) = \tau_3 \otimes \varepsilon_0(\mathbf{k})\sigma_0.$$
 (D6)

Therefore, along the (110) direction, the triplet-mixing Hamiltonian $H_0(\mathbf{k})$ has a nodal point at \mathbf{k} if and only if $\varepsilon_0(\mathbf{k}) = 0$. Since this a real equation on a 1D line, it is in general satisfied at a single-point node $\mathbf{k}_0(k_z)$ near $\mathbf{k}^s(k_z)$ at each k_z and thus extended line nodes are stable under triplet mixing as long as the symmetries M_z , \tilde{M}_{xy} are satisfied.

¹⁸If on the unlikely event that the $|\Delta_3|$ is sufficiently large so that Eq. (C3) never holds, there still exists a nodal point along the γ band since SOC is assumed to be zero for (C3).

4. Adding weak coupling between eigenspaces of $M_z = \pm i$

Let us fix k_z as before, and let \mathbf{k} be near $\mathbf{k}_0(k_z)$, but not necessarily in the (110) direction. Since $\mathrm{Sr}_2\mathrm{RuO}_4$ is quasi-2D, the coupling between eigenspaces of $M_z=\pm i$ must be weak and thus we can assume that $H(\mathbf{k})-H_0(\mathbf{k}_0)$ with respect to the gap of $H_0(\mathbf{k}_0)$ [lowest nonzero energy level of $H_0(\mathbf{k}_0)$ and not to be confused with the gap function $\Delta(\mathbf{k}_0)$] when \mathbf{k} is near \mathbf{k}_0 so that $P(\mathbf{k})$ can be well defined as the projection operator onto eigenstates of $H(\mathbf{k})$ with energies near zero and also unitarily equivalent to $P_0(\mathbf{k}_0)$ as explained in Appendix D 6. By perturbation theory (Weyl's inequality), the variation of the energy values must be small and thus it is sufficient to consider the restriction of $H_0(\mathbf{k})$ to $P_0(\mathbf{k})$ when attempting find the zero energies of $H_0(\mathbf{k})$, i.e., only eigenstates in $P_0(\mathbf{k})$ have energies sufficiently close to zero.

I. First assume that \mathbf{k} is still along the (110) direction so that \tilde{M}_{xy} is a local symmetry. It should be noted from the matrix form of \tilde{M}_{xy} with respect to $\{\phi_0(\mathbf{k}_0)\}$ in Eq. (D5) that

$$\operatorname{tr}(\tilde{M}_{xy}P_0(\mathbf{k}_0)) = 0. \tag{D7}$$

Since \tilde{M}_{xy} has eigenvalue ± 1 , we see that $\operatorname{tr}(\tilde{M}_{xy}P_0(\mathbf{k}_0))$ must be an integer and thus, by continuity, for sufficiently small variations $H(\mathbf{k}) - H_0(\mathbf{k}_0)$, we must also have

$$\operatorname{tr}(\tilde{M}_{xv}P(\mathbf{k})) = 0. \tag{D8}$$

Since $H_0(\mathbf{k})$ still preserves mirror symmetry \tilde{M}_{xy} in the diagonal planes and dim $P(\mathbf{k}) = \dim P_0(\mathbf{k}_0) = 4$, we see that eigenstates of $H(\mathbf{k})$ in $P(\mathbf{k})$ can be divided by the eigenspaces of $\tilde{M}_{xy} = \pm 1$, each of which is of dim 2, i.e., dim ker($\tilde{M}_{xy} \pm 1$) = 2. Notice that \mathcal{CP} commutes with \tilde{M}_{xy} and thus maps within each eigenspace $\tilde{M}_{xy} = \pm 1$. Hence, by Lemma 1, there exists an orthonormal basis χ_{\pm} , $\mathcal{CP}\chi_{\pm}$ consisting of eigenstates of $H(\mathbf{k})$ within each eigenspace $\tilde{M}_{xy} = \pm 1$, respectively. Let us now define

$$\phi(\mathbf{k}) = \frac{1}{\sqrt{2}}(\chi_+ + \chi_-).$$
 (D9)

Then it is clear that $\{\phi(\mathbf{k})\}$ forms a complete orthonormal basis for $P(\mathbf{k})$. We can then repeat the same argument as before, restricting to the effective two-band Hamiltonian $H(\mathbf{k})P(\mathbf{k})$, but only using mirror symmetry \tilde{M}_{xy} this time. In this case, we see that $\hat{\Delta}(\mathbf{k}) = 0$ while $\hat{\varepsilon}(\mathbf{k}) = \varepsilon(\mathbf{k})\sigma_0 + \varepsilon'(\mathbf{k})\sigma_1$ or, equivalently,

$$H(\mathbf{k})P(\mathbf{k}) = \tau_3 \otimes [\varepsilon(\mathbf{k})\sigma_0 + \varepsilon'(\mathbf{k})\sigma_1]. \tag{D10}$$

Therefore, the perturbed Hamiltonian $H(\mathbf{k})$ has a node if and only if $|\varepsilon(\mathbf{k})| = |\varepsilon'(\mathbf{k})|$. Since this we can either take $\varepsilon(\mathbf{k}) = +\varepsilon'(\mathbf{k})$ or $\varepsilon(\mathbf{k}) = -\varepsilon'(\mathbf{k})$, the originally single node \mathbf{k}_0 for H_0 splits into two nodes along the (110) direction for $H(\mathbf{k})$ and thus suggests that there exists a Bogliubov Fermi surface circling the original node \mathbf{k}_0 and intersecting the diagonal plane at the two nodes.

II. To check this, let us assume the general case where \mathbf{k} is not necessarily along the (110) direction, but still near the original node \mathbf{k}_0 . A similar argument can be repeated to show that there exists a complete basis $\{\phi(\mathbf{k}), \chi'(\mathbf{k}), \mathcal{CP}\phi(\mathbf{k}), \mathcal{CP}\chi(\mathbf{k})\}$ for $P(\mathbf{k})$, where $\phi(\mathbf{k}), \chi(\mathbf{k})$ are not related by mirror symmetry \tilde{M}_{xy} anymore. However, since \mathcal{CP} is still preserved, the effective two-band gap func-

tion $\hat{\Delta}(\mathbf{k})$ must form a singlet between the pseudospins, i.e., $\hat{\Delta}(\mathbf{k}) = \Delta(\mathbf{k})(i\sigma_2)$. This implies that the particle-hole dispersion relation $\hat{\epsilon}(\mathbf{k})$ can be unitarily transformed via any SU(2) rotation in pseudospin space without affecting the gap function. Therefore, the effective two-band Hamiltonian $H(\mathbf{k})P(\mathbf{k})$ can be unitarily transformed so that $\hat{\epsilon}(\mathbf{k})$ is diagonal with entries $\epsilon_{\pm}(\mathbf{k})$, i.e.,

$$H(\mathbf{k})P(\mathbf{k}) = \begin{pmatrix} \varepsilon_{+}(\mathbf{k}) & \Delta(\mathbf{k}) \\ & \varepsilon_{-}(\mathbf{k}) & -\Delta(\mathbf{k}) \\ & -\Delta(\mathbf{k})^{*} & -\varepsilon_{+}(\mathbf{k}) \\ & & -\varepsilon_{-}(\mathbf{k}) \end{pmatrix},$$
(D11)

where the solid lines divide the particle and hole subspaces. Therefore, the effective Hamiltonian $H(\mathbf{k})P(\mathbf{k})$ has a zero mode if and only

$$|\Delta(\mathbf{k})|^2 + \varepsilon_+(\mathbf{k})\varepsilon_-(\mathbf{k}) = 0.$$
 (D12)

In the absence of mirror symmetries and TRS, a small Zeeman splitting occurs in pseudospin space, i.e., $\varepsilon_+(\mathbf{k}) \neq \varepsilon_-(\mathbf{k})$, and thus a Bogoliubov FS is generated where Eq. (D12) is satisfied.

5. Some useful exact statements regarding symmetries

Lemma 1. Let A be a Hermitian operator on a 2N-dimensional Hilbert space and \mathcal{T} be an antiunitary operator which anticommutes with A and satisfies $\mathcal{T} = \mathcal{T}^{\dagger} = \mathcal{T}^{-1}$. Then there exists an orthonormal basis of the form ϕ_i , $\mathcal{T}\phi_i$, $i = 1, 2, \ldots, N$ where ϕ_i corresponds to eigenvalue a_i and $\mathcal{T}\phi_i$ corresponds to eigenvalue $-a_i$. In particular,

$$\dim \ker A \in 2\mathbb{N}.$$
 (D13)

Proof. It is clear that if ϕ is an eigenstate of eigenvalue a, then $\mathcal{T}\phi$ is an eigenstate of eigenvalue -a. Therefore, if $a \neq 0$, then ϕ , $\mathcal{T}\phi$ must be orthogonal, and thus the summation of all eigenspaces with nonzero eigenvalue $a \neq 0$ must be of even dimension. Since the total Hilbert space is 2N dimensions, we see that dim ker $A \in 2\mathbb{N}$. Let us now consider the restriction \mathcal{T}_A of \mathcal{T} to ker A. Since $\mathcal{T}_A^2 = I_A$ is the identity operator on ker A, we see that $(\mathcal{T}_A - I_A)(\mathcal{T} + I_A) = 0$. Hence, if $\phi \in \ker A$, then either $\tilde{\phi} \equiv (\mathcal{T}_A + I_A)\phi$ is nonzero and thus an eigenstate of \mathcal{T}_A with eigenvalue +1, OR $\tilde{\phi} = 0$ and thus ϕ is an eigenstate of \mathcal{T}_A with eigenvalue +1. In the latter case, we see that $i\phi$ is an eigenstate of \mathcal{T}_A with eigenvalue +1 since \mathcal{T}_A is antilinear. Hence, we can always find an orthonormal basis $\chi_1, \ldots, \chi_{2m}$ for ker A of eigenstates of \mathcal{T}_A with eigenvalue +1. Now let us define

$$\phi_{2i-1/2i} = \frac{1}{\sqrt{2}}(\chi_{2i-1} \pm i\chi_{2i}), \quad i = 1, 2, \dots, m.$$
 (D14)

Then it is clear that $\phi_{2i} = \mathcal{T}\phi_{2i-1}$ and thus we have found a basis of the form ϕ , $\mathcal{T}\phi$ for ker A and consequently for the entire Hilbert space.

Theorem 1. If BCS Hamiltonian h commutes with M_z , \tilde{M}_{xy} , then

$$\dim \ker h = 4m, \quad m \geqslant 0. \tag{D15}$$

More specifically, there exists an orthonormal basis for $\ker h$ of the form

$$\{\phi\} \equiv (\phi_i, \tilde{M}_{xy}\phi_i, \mathcal{CP}\phi, \mathcal{CP}\tilde{M}_{xy}\phi_i : i = 1, \dots, m).$$
 (D16)

Proof. Since h commutes with M_z and M_z is Hermitian with $M_{\tau}^2 = -1$, we can decompose the particle-hole subspace into the eigenspaces of $M_z = \pm i$. Notice that \mathcal{CP} commutes with M_z and since the eigenvalue of M_z are imaginary, we see that \mathcal{CP} is an antiunitary operator between the eigenspaces $M_z = +i \leftrightarrow M_z = -i$. In particular, we see that dim ker $(M_z \pm i) = 2n$. Since h anticommutes with \mathcal{CP} , we see that if ϕ is an eigenstate of h in eigenspace $M_z = +i$ with energy E, then $\mathcal{CP}\phi$ is an orthogonal eigenstate of h in eigenspace $M_z = -i$ with energy -E, and vice versa. Similarly, notice that \tilde{M}_{xy} anticommutes with M_z and thus is a unitary operator which maps between the eigenspaces $M_z = +i \leftrightarrow M_z = -i$. Therefore, \mathcal{CPM}_{xy} is an antiunitary map which maps each eigenspace onto itself, i.e., $ker(M_z \pm i)$ is invariant under $\mathcal{CP}\tilde{M}_{xy}$. Notice that $\mathcal{CP}\tilde{M}_{xy}$ is an antiunitary Hermitian operator which anticommutes with h within each eigenspace $ker(M_z \pm i)$. Therefore, by Lemma 1, within each eigenspace $ker(M_z \pm i)$, the kernel of h is doubly degenerate. In fact, we can find an orthonormal basis of the form ϕ_i , $\mathcal{CP}\tilde{M}_{xy}\phi_i$, $i=1,\ldots,m$, for $\ker h \cap \ker(\mathcal{M}_z-i)$ (notice that the basis may be empty, i.e., m = 0, if ker h is trivial, i.e., only contains the zero eigenstate). And by \mathcal{CP} symmetry, we see that the kernel of h is quartic degenerate. More specifically, ϕ_i , $\tilde{M}_{xy}\phi_i$, $\mathcal{CP}\phi_i$, $\mathcal{CP}\tilde{M}_{xy}\phi_i$, with $i=1,\ldots,m$, form an orthonormal basis for ker h.

6. The Riesz projector and perturbation theory

For this section, let h_0 be a Hermitian operator on a finite N-dimensional Hilbert space and let $h_{\lambda} = h_0 + \lambda V$ denote the perturbed Hermitian operator parametrized by the small parameter λ and the perturbation is denoted by V. To have a controlled perturbation theory, we require the eigenspaces of h_0 to "evolve smoothly" to those of h_{λ} as we tune the small parameter λ . One way of defining such a smooth evolution rigorously is to apply the Riesz projector [50,51], which we shall define shortly.

For simplicity, let $E^1(h_\lambda) \leqslant E^2(h_\lambda) \leqslant \cdots \leqslant E^N(h_\lambda)$ denote the eigenenergies of h_λ in ascending order (where each energy level is repeated by their degeneracy), and let E_0 denote a (possibly degenerate) eigenenergy of h_0 , i.e., there exists some i such that

$$E^{i-1}(h_0) < E_0 \equiv E^i(h_0) = E^{i+1}(h_0) \dots$$

= $E^{i+m-1}(h_0) < E^{i+m}(h_0).$ (D17)

It is then clear that we can draw a circle Γ in the complex plane $\mathbb C$ which only contains E_0 in the interior and none of the remaining energy levels of H_0 . By the Weyl inequality, we know that $|E^n(h_\lambda) - E^n(h_0)| \leq |\lambda| ||V||$, i.e., the variation in energy levels is controlled by the small parameter λ . Therefore, for sufficiently small λ , the energies $E^i(h_\lambda), \ldots, E^{i+m-1}(h_\lambda)$ are still contained in the interior of Γ while the remaining energy levels of h_λ are in the exterior. Within this neighborhood of λ

values, we can define the Riesz projector as

$$P_{\lambda} \equiv \frac{1}{2\pi i} \oint_{\Gamma} \frac{dz}{z - h_{\lambda}}.$$
 (D18)

It is then easy to see that P_{λ} is smooth with respect to λ and is equal to the projection operator onto the summation of eigenspaces $E^{i}(h_{\lambda}), \ldots, E^{i+m-1}(h_{\lambda})$. Since the number of energy levels (repeated by their degeneracy) does not change in the interior of Γ for sufficiently small λ , we see that dim P_{λ} is constant and $P_{\lambda}, P_{\lambda'}$ are unitarily equivalent for distinct values of small λ, λ' .

APPENDIX E: DECOMPOSITION OF THE INTERACTION

Consider the interaction \mathcal{V} in Eq. (9) given by the form $V(\mathbf{k} - \mathbf{k}')$ where we have suppressed the band indices μ , μ' for simplicity. Since $V(\mathbf{q})$ is assumed to be D_4 invariant, we can rewrite it in terms of *s*-wave lattice harmonics with range $R \geqslant 0$,

$$V(\mathbf{q}) = \sum_{R>0} v(R) S_R(\mathbf{q}). \tag{E1}$$

Let $|\mathbf{r}\rangle$ denote the Dirac delta function at real-space lattice site \mathbf{r} and W_R denote the D_4 -invariant subspace spanned by $|\mathbf{r}\rangle$ over all lattice sites \mathbf{r} of range R, i.e., $|\mathbf{r}| = R$. Then in real space, the lattice harmonic s_R can be written as the summation over all lattice sites \mathbf{r} of range R, i.e.,

$$S_R = \frac{1}{\sqrt{|W_R|}} \sum_{|\mathbf{r}|=R} |\mathbf{r}\rangle, \tag{E2}$$

$$S_R(\mathbf{r}) = \frac{1}{\sqrt{|W_R|}} \delta_{|\mathbf{r}|=R}, \tag{E3}$$

where $|W_R|$ is the number of lattice sites **r** with range *R*. Conversely, in momentum *k* space, the lattice harmonic can be rewritten as

$$s_R(\mathbf{k} - \mathbf{k}') = \frac{1}{\sqrt{|W_R|}} \sum_{|\mathbf{r}| = R} \langle \mathbf{k} - \mathbf{k}' | \mathbf{r} \rangle$$
 (E4)

$$= \frac{1}{\sqrt{|W_R|}} \sum_{|\mathbf{r}|=R} \langle \mathbf{k} | \mathbf{r} \rangle \langle \mathbf{r} | \mathbf{k}' \rangle$$
 (E5)

$$= \frac{1}{\sqrt{|W_R|}} \langle \mathbf{k} | \left[\sum_{|\mathbf{r}|=R} |\mathbf{r}\rangle \langle \mathbf{r}| \right] |\mathbf{k}'\rangle$$
 (E6)

$$= \frac{1}{\sqrt{|W_R|}} \langle \mathbf{k} | P_R | \mathbf{k}' \rangle, \tag{E7}$$

where P_R denotes the projection operator onto W_R . Notice that for a given range R, the subspace W_R can be decomposed into a unique combination of irreps of the symmetry group D_4 , and thus P_R must be diagonal in terms of its decomposition, i.e.,

$$P_R = \frac{1}{\sqrt{W_R}} \sum_{\psi_R} |\psi_R\rangle\langle\psi_R|, \tag{E8}$$

where the summation is over all possible lattice harmonics ψ_R in W_R corresponding to distinct irreps. In particular,

$$s_R(\mathbf{k} - \mathbf{k}') = \langle \mathbf{k} | P_R | \mathbf{k}' \rangle = \frac{1}{\sqrt{W_R}} \sum_{\psi_R} \psi_R(\mathbf{k}) \psi_R(\mathbf{k}')^*.$$
 (E9)

As an example, consider the case R = 1 in Table III. Since only $W_1 = A_1 \oplus B_1 \oplus E$, we see that

$$S_1(\mathbf{k} - \mathbf{k}') = \frac{1}{2} [S_1(\mathbf{k})S_1(\mathbf{k}') + D_1(\mathbf{k})D_1(\mathbf{k}')]$$

+ $\frac{1}{2} [p_x(\mathbf{k})p_x(\mathbf{k}') + p_y(\mathbf{k})p_y(\mathbf{k}')],$ (E10)

where $p_x(\mathbf{k})$, $p_y(\mathbf{k})$ is an orthonormal basis for the E irrep in W_1 . Notice that the terms projecting into the E irrep are not involved in computing the nonlinear gap equation in Eq. (11) since we assumed that the gap function Δ is of even parity. Therefore, in the main text, lattice harmonics belonging to the E irrep for any range R are omitted.

APPENDIX F: DIAGONALIZATION OF TWO-BAND BCS HAMILTONIAN: $SU(4) \rightarrow SO(6)$

1. Setup

Ignoring spin-orbit coupling, $\varepsilon_{SOC}(\mathbf{k}) = 0$, the two-band system involving the α , β bands decouples from the single- γ band in the BCS Hamiltonian. Therefore, we can use the reduced two-band Nambu spinor [in contrast to the three-band spinor in Eq. (3)]

$$\Psi^{\dagger}(\mathbf{k}) = [\psi_{x\uparrow}^{\dagger}(\mathbf{k}) \quad \psi_{y\uparrow}^{\dagger}(\mathbf{k}) \mid -\psi_{x\downarrow}(-\mathbf{k}) \quad -\psi_{y\downarrow}(-\mathbf{k})].$$
(F1)

To rewrite the decoupled two-band BCS Hamiltonian,

$$H(\mathbf{k}) = \begin{pmatrix} \varepsilon_{x} & \varepsilon_{h} & \Delta_{x} & \Delta_{h} \\ \varepsilon_{h} & \varepsilon_{y} & \Delta_{h} & \Delta_{y} \\ \Delta_{x}^{\dagger} & \Delta_{h}^{\dagger} & -\varepsilon_{x} & -\varepsilon_{h} \\ \Delta_{h}^{\dagger} & \Delta_{y}^{\dagger} & -\varepsilon_{h} & -\varepsilon_{y} \end{pmatrix}, \tag{F2}$$

where we have kept the **k** dependency implicit in the entries since the BCS Hamiltonian $H(\mathbf{k})$ is local in **k**, and the solid lines separate the particle-hole subspaces. Due to particle-hole symmetry and even parity, the eigenenergies of the local $H(\mathbf{k})$ are doubly degenerate, i.e., of the form $\pm E$. To reduce this degeneracy and make the diagonalization process more transparent, let us consider $H(\mathbf{k})^2$, i.e.,

$$H(\mathbf{k})^{2} = \begin{pmatrix} R+h & a+ib & 0 & c+id \\ a-ib & R-h & -c-id & 0 \\ \hline 0 & -c+id & R+h & a-ib \\ c-id & 0 & a+ib & R-h \end{pmatrix}$$
(F3)

$$= R + h\sigma_{03} + a\sigma_{01} - b\sigma_{32} - c\sigma_{22} - d\sigma_{12}.$$
 (F4)

where $\sigma_{\mu\nu}=\sigma_{\mu}\otimes\sigma_{\nu}$ is the tensor product of Pauli matrices and

$$R = \varepsilon_h^2 + |\Delta_h|^2 + \frac{1}{2} \left(\varepsilon_x^2 + |\Delta_x|^2 + \varepsilon_y^2 + |\Delta_y|^2 \right), \tag{F5}$$

$$h = \frac{1}{2} \left(\varepsilon_x^2 + |\Delta_x|^2 - \varepsilon_y^2 - |\Delta_y|^2 \right), \tag{F6}$$

$$a + ib = \Delta_h^{\dagger} \Delta_x + \Delta_h \Delta_v^{\dagger} + \varepsilon_h (\varepsilon_x + \varepsilon_v), \tag{F7}$$

$$c + id = \Delta_h(\varepsilon_x - \varepsilon_y) - (\Delta_x - \Delta_y)\varepsilon_h.$$
 (F8)

Indeed, to solve the nonlinear gap equation, we need to obtain the one-particle density matrix (1-pdm) $\Gamma(\mathbf{k})$ [52]

defined by

$$\Gamma(\mathbf{k}) \equiv \frac{1}{e^{\beta H(\mathbf{k})} + 1}$$

$$= \frac{1}{2} - H(\mathbf{k})U(\mathbf{k})^{\dagger} \frac{1}{2|\mathcal{E}(\mathbf{k})|} \tanh\left(\frac{\beta|\mathcal{E}(\mathbf{k})|}{2}\right)U(\mathbf{k}),$$
(F10)

where $U(\mathbf{k})$ is the unitary matrix which diagonalizes $H(\mathbf{k})^2$ into $\mathcal{E}(k)^2$. Notice that the 1-pdm $\Gamma(k)$ is related to the Nambu spinors in Eq. (F1) in the sense that the matrix entries of $\Gamma(\mathbf{k})$ are given by

$$\Gamma(\mathbf{k})_{ab} = \langle \Psi^{\dagger}(\mathbf{k})_b \Psi(\mathbf{k})_a \rangle. \tag{F11}$$

2. A reformulation of $SU(2) \rightarrow SO(3)$

The single-band BCS Hamiltonian is generally diagonalized via the $SU(2) \to SO(3)$ relation [or $\mathfrak{su}(2) \leftrightarrow \mathfrak{so}(3)$ isomorphism] and thus it is natural to think the corresponding $SU(4) \to SO(6)$ homomorphism [$\mathfrak{su}(4) \leftrightarrow \mathfrak{so}(6)$] can be used to diagonalize the two-band BCS Hamiltonian. With that in mind, let us reformulate the $SU(2) \to SO(3)$ relation so that it can be easily generalized to the $SU(4) \to SO(6)$ isomorphism.

Let $\hat{a} \wedge \hat{b}$ be the antisymmetric matrix with entry -1 at (a, b) and +1 as (b, a). In the example of d = 3 dimensions,

$$\hat{1} \wedge \hat{2} = -iL_3,\tag{F12}$$

$$\exp(\theta \hat{1} \wedge \hat{2}) = \exp(-i\theta L_3), \tag{F13}$$

where L_3 is the standard angular momentum along the $+\hat{3}$ direction. Notice that in d=3 dimension, a rotation in a plan (e.g., $e^{-i\theta L_3}$) can be specified by the normal vector $\hat{3}$ and a rotation angle θ . However, in higher dimensions, this is impossible and thus we instead specify a rotation by the plane, e.g., $\hat{1} \wedge \hat{2}$ (the plane spanned by the orthonormal frame $\hat{1}, \hat{2}$), and the rotation angle θ . Notice that $\hat{1} \wedge 2 = -\hat{2} \wedge \hat{1}$, and thus the order of the 2 axes represent the direction of rotation, e.g., $\exp(\theta \hat{1} \wedge \hat{2})$ rotates the axes $\hat{1} \rightarrow \hat{2}$ by an angle of θ .

It's then clear that the $SU(2) \rightarrow SO(3)$ relation [$\mathfrak{su}(2) \leftrightarrow \mathfrak{so}(3)$ isomorphism] is given by

$$\frac{1}{2i}\sigma_1 \leftrightarrow \hat{2} \land \hat{3},\tag{F14}$$

$$\frac{1}{2i}\sigma_2 \leftrightarrow \hat{3} \wedge \hat{1},\tag{F15}$$

$$\frac{1}{2i}\sigma_3 \leftrightarrow \hat{1} \wedge \hat{2},$$
 (F16)

where σ_i are the Pauli matrices. In particular, a 2×2 Hermitian matrix in the Lie algebra $i\mathfrak{su}(2)$

$$H = \cos\theta\sigma_3 + \sin\theta\sigma_1 \leftrightarrow \cos\theta\hat{1} \wedge \hat{2} + \sin\theta\hat{2} \wedge \hat{3} \quad (F17)$$

can be diagonalized $H = U^{\dagger} \sigma_3 U$ via the unitary operator

$$U = \exp\left(-\theta \frac{\sigma_2}{2i}\right) \leftrightarrow \exp(\theta \hat{3} \wedge \hat{1}). \tag{F18}$$

It should be emphasized that the only requirement for such a diagonalization procedure is that $\hat{1}$, $\hat{2}$, $\hat{3}$ form an orthonormal frame. In higher dimensions, such an orthonormal frame may

TABLE VI. SU(4) \rightarrow SO(6) relation. $\hat{1}$, $\hat{2}$, $\hat{3}$, $\hat{1}'$, $\hat{2}'$, $\hat{3}'$ denote the 6 axes generating \mathbb{R}^6 so that $\hat{a} \wedge \hat{b}$ generates the Lie algebra $\mathfrak{so}(6)$. The entry $\hat{a} \wedge \hat{b}$ in row μ and column ν corresponds to $\sigma_{\mu\nu}/2i$ where $\sigma_{\mu\nu} = \sigma_{\mu} \otimes \sigma_{\nu}$ is the tensor product of Pauli matrices, e.g., $\sigma_{13}/2i \leftrightarrow \hat{1}' \wedge \hat{3}$. The red boxes show the only nonzero entries in $H(\mathbf{k})^2$ in Eq. (F4).

	0	1	2	3	
0		$2 \wedge 3$	$\hat{3} \wedge \hat{1}$	$1 \wedge 2$	
1	$\hat{2}' \wedge \hat{3}'$	$\hat{1}' \wedge \hat{1}$		$1' \wedge \hat{3}$	(F19)
2	$\hat{3}' \wedge \hat{1}'$	$\hat{2}' \wedge \hat{1}$	$\hat{2}' \wedge \hat{2}$	$\hat{2}' \wedge \hat{3}$	
3	$\hat{1}' \wedge \hat{2}'$	$\hat{3}' \wedge \hat{1}$	$\hat{3}' \wedge \hat{2}$	$\hat{3}' \wedge \hat{3}$	

be arbitrarily chosen, and may not correspond to the original standard axes.

3. The $SU(4) \rightarrow SO(6)$ relation and its application to the two-band system

Using the framework established in the previous section, we can easily generalize the isomorphism to SU(4) \rightarrow SO(6), tabulated in Table VI. Indeed, let $\hat{1}, \hat{2}, \hat{3}, \hat{1}', \hat{2}', \hat{3}'$ denote the 6 axes generating \mathbb{R}^6 so that $\hat{a} \wedge \hat{b}$ generates the Lie algebra $\mathfrak{so}(6)$. Let $\sigma_{\mu\nu} = \sigma_{\mu} \otimes \sigma_{\nu}$ denote the tensor product of Pauli matrices (all except σ_{00}) which generates the Lie algebra $i\mathfrak{su}(4)$. Then Table VI is read in the following manner: the entry $\hat{a} \wedge \hat{b}$ in row μ and column ν corresponds to $\sigma_{\mu\nu}/2i$, e.g., $\sigma_{13}/2i \leftrightarrow \hat{1}' \wedge \hat{3}$.

To apply this isomorphism in diagonalizing the two-band system, notice that the red lines in Table VI boxes the only entries occurring in $H(\mathbf{k})^2$ as given in Eq. (F4). Therefore, we can map $H(\mathbf{k})^2$ into the Lie algebra $\mathfrak{so}(6)$ so that

$$H(\mathbf{k})^2 \leftrightarrow h\hat{1} \wedge \hat{2} + g\hat{2} \wedge \hat{n}$$
 (F20)

$$\leftrightarrow r(\cos\theta\,\hat{1}\,\wedge\,\hat{2} + \sin\theta\,\hat{2}\,\wedge\,\hat{n}),\tag{F21}$$

where we have ignored that constant *R* term since is commutes with any unitary operator and

$$g\hat{n} = a\hat{3} + b\hat{3}' + c\hat{2}' + d\hat{1}', \quad r^2 = h^2 + g^2.$$
 (F22)

It is then clear that $\hat{1}, \hat{2}, \hat{n}$ form an orthonormal frame in \mathbb{R}^6 , and thus using the example given in Eq. (F17), it is intuitive to see that $H(\mathbf{k})^2$ is diagonalized via

$$U(\mathbf{k}) \leftrightarrow \exp\left(\theta \hat{n} \wedge \hat{1}\right) \tag{F23}$$

$$= \exp\left(i\frac{\theta}{2g}(a\sigma_{02} + b\sigma_{31} + c\sigma_{21} + d\sigma_{11})\right)$$
 (F24)

$$= \cos\left(\frac{\theta}{2}\right) + i \sin\left(\frac{\theta}{2}\right) \frac{1}{g} (a\sigma_{02} + b\sigma_{31} + c\sigma_{21} + d\sigma_{11})$$

(F25)

so that

$$H(\mathbf{k})^2 = U(\mathbf{k})^{\dagger} \mathcal{E}(\mathbf{k})^2 U(\mathbf{k}), \quad \mathcal{E}(\mathbf{k})^2 = R + r\sigma_{03}.$$
 (F26)

In particular, there exists $F(\mathbf{k})$, $f(\mathbf{k})$ given by

$$F(\mathbf{k}) = \sum_{\sigma=\pm} \frac{1}{4\sqrt{R(\mathbf{k}) + \sigma r(\mathbf{k})}} \tanh\left(\frac{\beta}{2}\sqrt{R(\mathbf{k}) + \sigma r(\mathbf{k})}\right),$$
(F27)

$$f(\mathbf{k}) = \sum_{\sigma = \pm} \frac{\sigma}{4\sqrt{R(\mathbf{k}) + \sigma r(\mathbf{k})}} \tanh\left(\frac{\beta}{2}\sqrt{R(\mathbf{k}) + \sigma r(\mathbf{k})}\right),$$
(F28)

such that

$$\frac{1}{2|\mathcal{E}(\mathbf{k})|}\tanh\left(\frac{\beta|\mathcal{E}(\mathbf{k})|}{2}\right) = F(\mathbf{k}) + f(\mathbf{k})\sigma_{03},\tag{F29}$$

$$U(\mathbf{k})^{\dagger} \frac{1}{2|\mathcal{E}(\mathbf{k})|} \tanh\left(\frac{\beta|\mathcal{E}(\mathbf{k})|}{2}\right) U(\mathbf{k})$$

$$= F(\mathbf{k}) + \frac{f(\mathbf{k})}{r(\mathbf{k})} \begin{pmatrix} h & a+ib & 0 & c+id \\ a-ib & -h & -c-id & 0 \\ \hline 0 & -c+id & +h & a-ib \\ c-id & 0 & a+ib & -h \end{pmatrix}$$
(F30)

$$= F(\mathbf{k}) + \frac{f(\mathbf{k})}{r(\mathbf{k})} [H(\mathbf{k})^2 - R(\mathbf{k})]. \tag{F31}$$

It is then easy to obtain the 1-pdm $\Gamma(\mathbf{k})$ in Eq. (F9).

APPENDIX G: SIMULATING STRAIN AND STRESS

In this Appendix, we describe the detailed parameters used to simulate pure A_1 and B_2 strain in the main text. For simplicity, let us define

$$\varepsilon_0 \equiv \frac{1}{2}(\varepsilon_x + \varepsilon_y),$$
 (G1)

$$\varepsilon_3 \equiv \frac{1}{2}(\varepsilon_x - \varepsilon_y),$$
 (G2)

where ε_0 , ε_3 should be regarded as the coefficients of decomposing the x, y band structure into Pauli matrices, i.e.,

$$\begin{pmatrix} \varepsilon_x & \varepsilon_h \\ \varepsilon_h & \varepsilon_y \end{pmatrix} = \varepsilon_0 \sigma_0 + \varepsilon_h \sigma_1 + \varepsilon_3 \sigma_3.$$
 (G3)

In the absence of strain, ε_x , ε_y are given by Eq. (A1) and thus we rewrite the equations as follows:

$$\varepsilon_0(\mathbf{k}) = -\mu_0 - 2t_0(\cos k_x + \cos k_y) + 4t_0' \sin k_x \sin k_y,$$

$$t_0 = (t_x + t_y)/2 \tag{G4}$$

$$\varepsilon_3(\mathbf{k}) = -2t_3(\cos k_x - \cos k_y) - 2t_3'(\cos k_x - \cos k_y),$$

$$t_3 = (t_x - t_y)/2$$
(G5)

$$\varepsilon_z(\mathbf{k}) = -\mu_z - 2t_z(\cos k_x + \cos k_y) - 2t_z'(2\cos k_x \cos k_y),$$
(G6)

$$\varepsilon_h(\mathbf{k}) = 4t_h \sin k_x \sin k_y. \tag{G7}$$

To simulate different types of strain, let us introduce the following notation:

$$\varepsilon_0(\mathbf{k}) = -\mu_{0,A_1} - 2t_{0,A_1}(\cos k_x + \cos k_y) - 2t_{0,B_1}(\cos k_x - \cos k_y) + 4t_{0,B_2}\sin k_x \sin k_y,$$
 (G8)

(G16)

$$\varepsilon_3(\mathbf{k}) = -2t_{3,A_1}(\cos k_x - \cos k_y) - 2t_{3,B_1}(\cos k_x + \cos k_y),$$

(G9)

$$\varepsilon_{z}(\mathbf{k}) = -\mu_{z,A_{1}} - 2t_{z,A_{1}}(\cos k_{x} + \cos k_{y}) - 2t'_{z,A_{1}}(2\cos k_{x}\cos k_{y})$$
 (G10)

$$-2t_{z,B_1}(\cos k_x - \cos k_y) + 4t_{z,B_2}\sin k_x \sin k_y, \quad (G11)$$

$$\varepsilon_h(\mathbf{k}) = 4t_{h,A_1} \sin k_x \sin k_y. \tag{G12}$$

To simulate pure A_1 strain ε_{A_1} , we have

$$t_{s,A_1}(\varepsilon_{A_1}) = t_s(1 - \alpha_{t,A_1}\varepsilon_{A_1}), \quad s = z, z', 0, 3, h$$
 (G13)

$$\mu_{z,A_1}(\varepsilon_{A_1}) = \mu_0(1 - \alpha_{\mu,A_1}\varepsilon_{A_1}),$$
 (G14)

where μ_{0,A_1} is modified so that the total density of electrons $\langle n \rangle$ is kept fixed for nonzero values of ε_{A_1} , and we have taken $\alpha_{t,A_1} = 3$ and $\alpha_{\mu,A_1} = 8$ so that we mainly modify the chemical potentials when simulating pure A_1 strain. Similarly, to simulate pure B_1 and B_2 strain, we have

$$t_{s,B_1}(\varepsilon_{B_1}) = -t_s \alpha_{B_1} \varepsilon_{B_1}, \quad s = z, 0, 3$$
 (G15)

where we have taken $\alpha_{B_1} = \alpha_{B_2} = 12$.

It should be noted that in order to simulate uniaxial stress, we used the Poisson ratio $\nu \approx 0.3935$ for Sr_2RuO_4 [53] so that both A_1 strain and B_1 strain are present, i.e.,

 $t_{s,B_2}(\varepsilon_{B_2}) = -t_3\alpha_{B_2}\varepsilon_{B_2}, \quad s = z, 0$

$$\varepsilon_{yy} = -\nu \varepsilon_{xx},$$
 (G17)

$$\varepsilon_{A_1} = \frac{1}{2}(\varepsilon_{xx} + \varepsilon_{yy}),$$
 (G18)

$$\varepsilon_{B_1} = \frac{1}{2}(\varepsilon_{xx} - \varepsilon_{yy}).$$
 (G19)

The magnitudes $\alpha_{t,A_1}, \alpha_{\mu,A_1}, \alpha_{B_1}$ were tuned¹⁹ so that the γ band in Sr_2RuO_4 crosses the Van Hove point at $\varepsilon_{xx} \approx -0.44\%$ [12], while the α , β bands distort slightly (an asymmetry of \sim 2%) [32].

¹⁹Notice that the magnitudes α are slightly different from the SI of Ref. [12]. Indeed, the reference only considered the single- γ band case and did not modify the chemical potential μ_z , which we believe to be the main source of A_1 strain since it first appears as an onsite hopping term.

- [1] A. P. Mackenzie and Y. Maeno, The superconductivity of Sr₂RuO₄ and the physics of spin-triplet pairing, Rev. Mod. Phys. 75, 657 (2003).
- [2] M. Sigrist, Review on the chiral p-wave phase of Sr₂RuO₄, Prog. Theor. Phys. Suppl. 160, 1 (2005).
- [3] Y. Maeno, S. Kittaka, T. Nomura, S. Yonezawa, and K. Ishida, Evaluation of spin-triplet superconductivity in Sr₂RuO₄, J. Phys. Soc. Jpn. 81, 011009 (2012).
- [4] C. Kallin, Chiral p-wave order in Sr₂RuO₄, Rep. Prog. Phys. 75, 042501 (2012).
- [5] A. P. Mackenzie, T. Scaffidi, C. W. Hicks, and Y. Maeno, Even odder after twenty-three years: The superconducting order parameter puzzle of Sr₂RuO₄, npj Quantum Mater. 2, 40 (2017).
- [6] A. P. Mackenzie, R. K. W. Haselwimmer, A. W. Tyler, G. G. Lonzarich, Y. Mori, S. Nishizaki, and Y. Maeno, Extremely Strong Dependence of Superconductivity on Disorder in Sr₂RuO₄, Phys. Rev. Lett. **80**, 161 (1998).
- [7] C. Lupien, W. A. MacFarlane, C. Proust, L. Taillefer, Z. Q. Mao, and Y. Maeno, Ultrasound Attenuation in Sr₂RuO₄: An Angle-Resolved Study of the Superconducting Gap Function, Phys. Rev. Lett. 86, 5986 (2001).
- [8] I. Bonalde, B. D. Yanoff, M. B. Salamon, D. J. Van Harlingen, E. M. E. Chia, Z. Q. Mao, and Y. Maeno, Temperature Dependence of the Penetration Depth in Sr₂RuO₄: Evidence for Nodes in the Gap Function, Phys. Rev. Lett. 85, 4775 (2000).
- [9] K. Ishida, M. Manago, K. Kinjo, and Y. Maeno, Reduction of the 170 Knight shift in the superconducting state and the heatup effect by NMR pulses on Sr₂RuO₄, J. Phys. Soc. Jpn. 89, 034712 (2020).
- [10] A. Pustogow, Y. Luo, A. Chronister, Y.-S. Su, D. A. Sokolov, F. Jerzembeck, A. P. Mackenzie, C. W. Hicks, N. Kikugawa, S. Raghu et al., Constraints on the superconducting order parameter in Sr₂RuO₄ from oxygen-17 nuclear magnetic resonance, Nature (London) 574, 72 (2019).

- [11] A. Chronister, A. Pustogow, N. Kikugawa, D. A. Sokolov, F. Jerzembeck, C. W. Hicks, A. P. Mackenzie, E. D. Bauer, and S. E. Brown, Evidence for even parity unconventional superconductivity in Sr₂RuO₄, Proc. Natl. Acad. Sci. USA 118, e2025313118 (2021).
- [12] Y.-S. Li, M. Garst, J. Schmalian, N. Kikugawa, D. A. Sokolov, C. W. Hicks, F. Jerzembeck, M. S. Ikeda, A. W. Rost, M. Nicklas et al., Elastocaloric determination of the phase diagram of Sr₂RuO₄, Nature (London) **607**, 276 (2022).
- [13] S. Ghosh, A. Shekhter, F. Jerzembeck, N. Kikugawa, D. A. Sokolov, M. Brando, A. P. Mackenzie, C. W. Hicks, and B. J. Ramshaw, Thermodynamic evidence for a two-component superconducting order parameter in Sr₂RuO₄, Nat. Phys. 17, 199 (2021).
- [14] S. Benhabib, C. Lupien, I. Paul, L. Berges, M. Dion, M. Nardone, A. Zitouni, Z. Q. Mao, Y. Maeno, A. Georges et al., Ultrasound evidence for a two-component superconducting order parameter in Sr₂RuO₄, Nat. Phys. 17, 194 (2021).
- [15] I. Žutić and I. Mazin, Phase-Sensitive Tests of the Pairing State Symmetry in Sr₂RuO₄, Phys. Rev. Lett. **95**, 217004 (2005).
- [16] S. Beck, A. Hampel, M. Zingl, C. Timm, and A. Ramires, Effects of strain in multiorbital superconductors: The case of Sr₂RuO₄, Phys. Rev. Res. 4, 023060 (2022).
- [17] A. Ramires, Nodal gaps from local interactions in Sr₂RuO₄, in Journal of Physics: Conference Series, Vol. 2164 (IOP Publishing, Bristol, 2022), p. 012002.
- [18] H. G. Suh, H. Menke, P. M. R. Brydon, C. Timm, A. Ramires, and D. F. Agterberg, Stabilizing even-parity chiral superconductivity in Sr₂RuO₄, Phys. Rev. Res. 2, 032023(R) (2020).
- [19] A. Ramires and M. Sigrist, Superconducting order parameter of Sr₂RuO₄: A microscopic perspective, Phys. Rev. B 100, 104501
- [20] S. Käser, H. U. Strand, N. Wentzell, A. Georges, O. Parcollet, and P. Hansmann, Interorbital singlet pairing in

- Sr₂RuO₄: A Hund's superconductor, Phys. Rev. B **105**, 155101 (2022).
- [21] A. T. Rømer, T. A. Maier, A. Kreisel, P. J. Hirschfeld, and B. M. Andersen, Leading superconducting instabilities in threedimensional models for Sr₂RuO₄, Phys. Rev. Res. 4, 033011 (2022).
- [22] S. A. Kivelson, A. C. Yuan, B. Ramshaw, and R. Thomale, A proposal for reconciling diverse experiments on the superconducting state in Sr₂RuO₄, npj Quantum Mater. 5, 43 (2020).
- [23] A. C. Yuan, E. Berg, and S. A. Kivelson, Strain-induced time reversal breaking and half quantum vortices near a putative superconducting tetracritical point in Sr₂RuO₄, Phys. Rev. B 104, 054518 (2021).
- [24] Y. Sheng, Y. Li, and Y.-F. Yang, Multipole-fluctuation pairing mechanism of $d_{x^2-y^2} + ig$ superconductivity in Sr_2RuO_4 , Phys. Rev. B **106**, 054516 (2022).
- [25] O. Gingras, N. Allaglo, R. Nourafkan, M. Côté, and A.-M. S. Tremblay, Superconductivity in correlated multiorbital systems with spin-orbit coupling: Coexistence of even-and odd-frequency pairing, and the case of Sr₂RuO₄, Phys. Rev. B 106, 064513 (2022).
- [26] J. Clepkens, A. W. Lindquist, and H.-Y. Kee, Shadowed triplet pairings in Hund's metals with spin-orbit coupling, Phys. Rev. Res. 3, 013001 (2021).
- [27] A. T. Rømer, A. Kreisel, M. A. Müller, P. J. Hirschfeld, I. M. Eremin, and B. M. Andersen, Theory of strain-induced magnetic order and splitting of T_c and T_{trsb} in Sr₂RuO₄, Phys. Rev. B 102, 054506 (2020).
- [28] A. T. Rømer, P. J. Hirschfeld, and B. M. Andersen, Super-conducting state of Sr₂RuO₄ in the presence of longer-range Coulomb interactions, Phys. Rev. B **104**, 064507 (2021).
- [29] V. Grinenko, S. Ghosh, R. Sarkar, J.-C. Orain, A. Nikitin, M. Elender, D. Das, Z. Guguchia, F. Brückner, M. E. Barber *et al.*, Split superconducting and time-reversal symmetry-breaking transitions in Sr₂RuO₄ under stress, Nat. Phys. 17, 748 (2021).
- [30] J. Xia, Y. Maeno, P. T. Beyersdorf, M. M. Fejer, and A. Kapitulnik, High Resolution Polar Kerr Effect Measurements of Sr₂RuO₄: Evidence for Broken Time-Reversal Symmetry in the Superconducting State, Phys. Rev. Lett. 97, 167002 (2006).
- [31] E. Hassinger, P. Bourgeois-Hope, H. Taniguchi, S. René de Cotret, G. Grissonnanche, M. S. Anwar, Y. Maeno, N. Doiron-Leyraud, and L. Taillefer, Vertical Line Nodes in the Superconducting Gap Structure of Sr₂RuO₄, Phys. Rev. X 7, 011032 (2017).
- [32] V. Sunko, E. Abarca Morales, I. Marković, M. E. Barber, D. Milosavljević, F. Mazzola, D. A. Sokolov, N. Kikugawa, C. Cacho, P. Dudin *et al.*, Direct observation of a uniaxial stress-driven Lifshitz transition in Sr₂RuO₄, npj Quantum Mater. 4, 46 (2019).
- [33] Y.-T. Hsu, W. Cho, A. F. Rebola, B. Burganov, C. Adamo, K. M. Shen, D. G. Schlom, C. J. Fennie, and E.-A. Kim, Manipulating superconductivity in ruthenates through Fermi surface engineering, Phys. Rev. B 94, 045118 (2016).
- [34] F. Jerzembeck, H. S. Røising, A. Steppke, H. Rosner, D. A. Sokolov, N. Kikugawa, T. Scaffidi, S. H. Simon, A. P. Mackenzie, and C. W. Hicks, The superconductivity of Sr₂RuO₄ under c-axis uniaxial stress, Nat. Commun. 13, 4596 (2022).
- [35] E. I. Blount, Symmetry properties of triplet superconductors, Phys. Rev. B 32, 2935 (1985).

- [36] E. Berg, C.-C. Chen, and S. A. Kivelson, Stability of Nodal Quasiparticles in Superconductors with Coexisting Orders, Phys. Rev. Lett. 100, 027003 (2008).
- [37] B. Béri, Topologically stable gapless phases of time-reversalinvariant superconductors, Phys. Rev. B 81, 134515 (2010).
- [38] S. Kobayashi, K. Shiozaki, Y. Tanaka, and M. Sato, Topological blount's theorem of odd-parity superconductors, Phys. Rev. B **90**, 024516 (2014).
- [39] The existence and stability of nodal behavior is often considered together, despite being separate issues. The main reason is that usually, in the presence (absence) of TRS, the determinant $\det H(\mathbf{k})$ can be reduced (i.e., remove the particle-hole degeneracy) to a complex function (real Pfaffian) for all momentum k. Existence can then be generally solved by finding the roots (setting = 0). Stability then follows from the continuity of the complex function (real Pfaffian) or by generating a topological invariant, i.e., a $\mathbb Z$ winding number (a $\mathbb Z_2$ invariant corresponding to real and negative values of the Pfaffian) [35–38]. However, when mirror symmetries are involved, the determinant can at most only be reduced along the mirror plane, where the existence of nodal points can be shown. Away from the mirror planes, but still near the nodal point, the reduction often breaks down and thus the stability has to be considered separately via perturbation theory. Indeed, in Appendix D, we prove that for general SCs, mirror symmetries \mathcal{M}_z , \mathcal{M}_{xy} are sufficient to stabilize nodal points (provided they exist) even when TRS is broken. However, the existence of such nodal points in the singlet d + ig state follows from the special property where gauge invariance can be applied (as discussed below).
- [40] D. F. Agterberg, P. M. R. Brydon, and C. Timm, Bogoliubov Fermi Surfaces in Superconductors with Broken Time-Reversal Symmetry, Phys. Rev. Lett. 118, 127001 (2017).
- [41] They both generate either $d_{x,y}$ or g-wave symmetry. The intuition (numerically justified) is that a sufficiently repulsive (positive) $v_{x,y}$ would imply that the SC order parameter changes sign between the x, y bands and thus preferring a g wave. The positive slope implies a repulsive (positive) $v_{z,z}$ and thus discourages the d_{xy} wave on the z band. Conversely, attractive (negative) $v_{x,y}$, $v_{z,z}$ would generate a d_{xy} wave on the x, y bands and z band, respectively.
- [42] T. Scaffidi, J. C. Romers, and S. H. Simon, Pairing symmetry and dominant band in Sr₂RuO₄, Phys. Rev. B 89, 220510(R) (2014).
- [43] D. F. Agterberg, T. M. Rice, and M. Sigrist, Orbital Dependent Superconductivity in Sr₂RuO₄, Phys. Rev. Lett. 78, 3374 (1997).
- [44] S. Raghu, A. Kapitulnik, and S. A. Kivelson, Hidden Quasi-One-Dimensional Superconductivity in Sr₂RuO₄, Phys. Rev. Lett. **105**, 136401 (2010).
- [45] J.-W. Huo, T. M. Rice, and F.-C. Zhang, Spin Density Wave Fluctuations and P-wave Pairing in Sr₂RuO₄, Phys. Rev. Lett. **110**, 167003 (2013).
- [46] I. A. Firmo, S. Lederer, C. Lupien, A. P. Mackenzie, J. C. Davis, and S. A. Kivelson, Evidence from tunneling spectroscopy for a quasi-one-dimensional origin of superconductivity in Sr₂RuO₄, Phys. Rev. B 88, 134521 (2013).
- [47] X. Wang, Z. Wang, and C. Kallin, Higher angular momentum pairing states in Sr₂RuO₄ in the presence of longer-range interactions, Phys. Rev. B **106**, 134512 (2022).

- [48] Y. Sidis, M. Braden, P. Bourges, B. Hennion, S. NishiZaki, Y. Maeno, and Y. Mori, Evidence for Incommensurate Spin Fluctuations in Sr₂RuO₄, Phys. Rev. Lett. 83, 3320 (1999).
- [49] B. Burganov, C. Adamo, A. Mulder, M. Uchida, P. D. C. King, J. W. Harter, D. E. Shai, A. S. Gibbs, A. P. Mackenzie, R. Uecker, M. Bruetzam, M. R. Beasley, C. J. Fennie, D. G. Schlom, and K. M. Shen, Strain Control of Fermiology and Many-Body Interactions in Two-Dimensional Ruthenates, Phys. Rev. Lett. 116, 197003 (2016).
- [50] T. Kato, Perturbation Theory for Linear Operators (Springer, Berlin, 2013), Vol. 132.
- [51] P. D. Hislop and I. M. Sigal, Introduction to Spectral Theory: With Applications to Schrödinger Operators (Springer, Berlin, 2012), Vol. 113.
- [52] V. Bach, E. H. Lieb, and J. P. Solovej, Generalized Hartree-Fock theory and the Hubbard model, J. Stat. Phys. **76**, 3 (1994).
- [53] J. Paglione, C. Lupien, W. A. MacFarlane, J. M. Perz, L. Taillefer, Z. Q. Mao, and Y. Maeno, Elastic tensor of Sr₂RuO₄, Phys. Rev. B 65, 220506(R) (2002).